Functional analysis of physical force during *Xenopus* gastrulation movements

Yusuke Hara

DOCTOR OF PHILOSOPHY

Department of Basic Biology

School of Life Science

The Graduate University for Advanced Studies

2013

Contents

Abbreviations

A-P: anterior-posterior

AM: axial mesoderm

BCR: blastocoel roof

CE: convergent extension

DMZ: dorsal marginal zone

ECM: extracellular matrix

FN: fibronectin

GFP: green fluorescence protein

LEM: leading edge mesoderm

memGFP: membrane-targeted green fluorescence protein

memRFP: membrane-targeted red fluorescence protein

MEMFA: MOPS-EGTA-$MgSO_4$-formaldehyde solution

MMR: Marc's modified ringers

MO: antisense Morpholino oligonucleotides

mRNA: messenger RNA

PCP: planer cell polarity

RFP: read fluorescence protein

RT: room temperature

RT-PCR: reverse transcription-polymerase chain reaction

St.: stage

VMZ: ventral marginal zone

List of Figures

Abstract

Gastrulation is a dynamic tissue-remodeling process occurring during early development and fundamental to the later organogenesis. It involves both chemical signals and physical factors. Although much is known about the molecular pathways involved, the roles of physical forces in regulating cellular behavior and tissue remodeling during gastrulation have just begun to be explored. Here, I characterized the force generated by the leading-edge mesoderm (LEM) that migrates preceding axial mesoderm (AM), and investigated the contribution of LEM during *Xenopus* gastrulation. First, I constructed an assay system using micro-needle which could measure physical forces generated by the anterior migration of LEM, and estimated the absolute magnitude of force generated by LEM (500 x 500 μm) using the micro-needle assay to be approximately 40 nN on average. Second, laser ablation experiments showed that LEM could affect the force distribution in the AM (i.e. LEM adds stretch force on axial mesoderm along anterior-posterior axis). Third, LEM was found to be necessary for the proper gastrulation cell movements and the establishment of organized notochord structure; a reduction of LEM migratory activity resulted in the disruption of mediolateral cell orientation and convergence in AM. Finally, I found that LEM migration cooperates with Wnt/PCP to form proper notochord. These results suggest that the force generated by the directional migration of LEM is transmitted to AM and supports the tissue organization of notochord regulated by Wnt/PCP in vivo. I propose that the LEM may have an additional regulatory role which aids the AM elongation through mechanical processes.

1. Introduction

1.1 Cells can sense, use, and generate physical forces

Physical forces are considerable regulatory factors of biological events which affect a broad range of cellular processes. Studies using cultured cells have shown that cells can sense various mechanical stresses such as tension, compression, shear stress, and environments of substrate through cell-ECM adhesions, cell-cell adhesions, membrane components, cytoskeletal components, and nuclei (Ingber, 2006). These mechanical stimuli affect essential cellular processes such as cell proliferation, differentiation, polarity, and migration (Engler et al., 2006; Fink et al., 2011; Ives et al., 1986; Klein et al., 2009; Lo et al., 2000; Neidlinger-Wilke et al., 2001). The mechanical inputs are translated into various biochemical signals by several ways, and this process called mechanotransduction is fundamental to biological and physiological events (Jaalouk and Lammerding, 2012). At the same time, cells can generate physical forces. To know the magnitude of generated force by a cell or multi cells, many measurement methods and techniques have been developed so far such as micro-pillar, traction force microscopy and atomic force microscopy (reviewed by Addae-Mensah and Wiksow, 2008). Using these techniques, various studies have estimated the traction force generated by a single cell and by a monolayer of cells as approximately 10-100 nN (Balaban et al., 2001; du Roure et al., 2005; Galbraith and Sheetz, 1997; Lee et al., 1994; Petronis et al., 2003; Tan et al., 2003; Tymchenko et al., 2007).

1.2 Involvement of the physical force in development

The study of mechano-responsibility and force measurement using the cultured cells is definitely important. However, the in vitro analyses with cultured cell are not able to

answer to questions as to how the forces are utilized for developmental and physiological events and how much force is actually exerted in embryos or animals in vivo.

Animal development involves successive cell movements and tissue rearrangements that transform a mass of embryonic cells into complex organ structures. Given that these dynamic events occur under the spatial constraint of the embryo size, it is thought that complex force fields exist in the embryos. In fact, in addition to molecular processes, physical forces have recently been shown to have essential functions in tissue morphogenesis and animal development (Lecuit et al., 2011; Mammoto and Ingber, 2010; Wozniak and Chen, 2009; Zhang and Labouesse, 2012). These reports strongly indicate that not only cells and tissues use forces but also actively moving/deforming cells and tissues can generate physical forces and affect the morphogenetic events of neighbor tissues in vivo. Therefore, the physical force is an unignorable factor to understand normal development.

For better and more precise understanding of animal development, an integrated analysis of tissue movements and characterization of morphogenetic events taking physical forces into account is certainly necessary. Thus, in this study, I attempted to address important questions regarding to force-involved processes in vivo, such as 1) which tissue generates the force, 2) how much force is generated during tissue movements, and 3) which tissue is affected by the generated force.

1.3.1 Model system: gastrulation

To attack those problems, I focused on the involvement of physical force in gastrulation process. Gastrulation is a dynamic process of tissue remodeling during early development in various kinds of animals (Solnica-Krezel and Sepich, 2012). During gastrulation, embryos undergo complex and dramatic cell shape changes and tissue rearrangements to form organs at the right time and location and to establish the proper body plan. Thus, it is reasonable to speculate that tissue movements occurring in gastrulation generate physical forces and such forces may play important roles for later morphogenesis of tissues and organs. The cell movements and molecular mechanisms involved in gastrulation have been extensively studied using *Xenopus laevis* (Keller, 2002; Keller et al., 2003; Wang and Steinbeisser, 2009). The *Xenopus* gastrula is thought to involve various physical factors (Davidson, 2011). In addition, *Xenopus* embryos are relatively large and easily handled for experimental manipulations, which are advantageous for measuring and applying physical forces, making the *Xenopus* gastrula an excellent model for addressing the above questions.

1.3.2 Leading-edge mesoderm of *Xenopus* gastrula

In this study, I focused on a highly migratory mesodermal tissue, the leading-edge mesoderm (LEM; also known as “head mesoderm” or “anterior mesendoderm”) which shows directional migration toward the future anterior side during *Xenopus* gastrulation. The LEM consists of mesendodermal cells derived from the peripheral region of the blastocoel floor. The most dorsal region of LEM first attach to the underside of the blastocoel roof (BCR) by vegetal rotation in the early gastrula stage (Winklbauer and

Schurfeld, 1999) (Fig. 1-1, process 1, red). After contacting the BCR, the LEM does not converge and extend like the later-involuting axial mesoderm, but migrates collectively and unidirectionally toward the animal pole as a cell stream on a fibronectin (FN) substrate, which coats the inner surface of the BCR (Fig. 1-1, process 3), and then subsequent dorsal tissues invaginate (Boucaut and Darribere, 1983; Davidson et al., 2002; Lee et al., 1984; Winklbauer and Keller, 1996; Winklbauer and Nagel, 1991). The anterior migration of LEM is controlled by several chemoatractant molecules such as SDF-1 (stromal cell-derived factor-1), CXCR4, and PDGF (platelet-derived growth factor) (Fukui et al., 2007; Nagel et al., 2004). It has been generally thought that such collective cell migrations can generate and exert force on the trailing cells (Trepat et al., 2009). Therefore, I presumed that the actively moving LEM could generate physical force by its migration during *Xenopus* gastrulation and attempted to characterize the nature and biological significance of the force.

1.3.3 Axial mesoderm of *Xenopus* gastrula

I also focused on the axial mesoderm (AM) in this study. The AM is initially located at the dorsal marginal zone and after the onset of gastrulation, it follows the invaginating LEM (Fig. 1-1, process 2, yellow). After the involution, the AM cells elongate and extend protrusions mediolaterally to intercalate between one another during gastrulation, resulting in the mediolateral narrowing and anterior-posterior (A-P) lengthening of the embryo (Fig. 1-1, process 4); this process is called convergent extension (CE) (Keller et al., 2000; Shih and Keller, 1992a; Shih and Keller, 1992b; Tada and Heisenberg, 2012). CE is generally thought to be regulated by the signaling

pathway that is initiated by secreted Wnt ligands, which are essential for establishing planar cell polarity (PCP) (Wallingford et al., 2002). Through the activation of the Wnt receptor Frizzled by the ligands, RhoA and Rac1 GTPases, and regulators of cytoskeletal architecture are activated by Xdsh, the *Xenopus* orthologue of Dishevelled, a component of the Wnt/PCP signaling pathway, and these molecules play critical roles in regulating the cell polarity, and thus the mediolateral intercalation of AM occurs during *Xenopus* gastrulation (Habas et al., 2003; Habas et al., 2001; Tada and Heisenberg, 2012; Tahinci and Symes, 2003; Wallingford et al., 2000). Ultimately, the AM forms the notochord and contribute to A-P axis elongation.

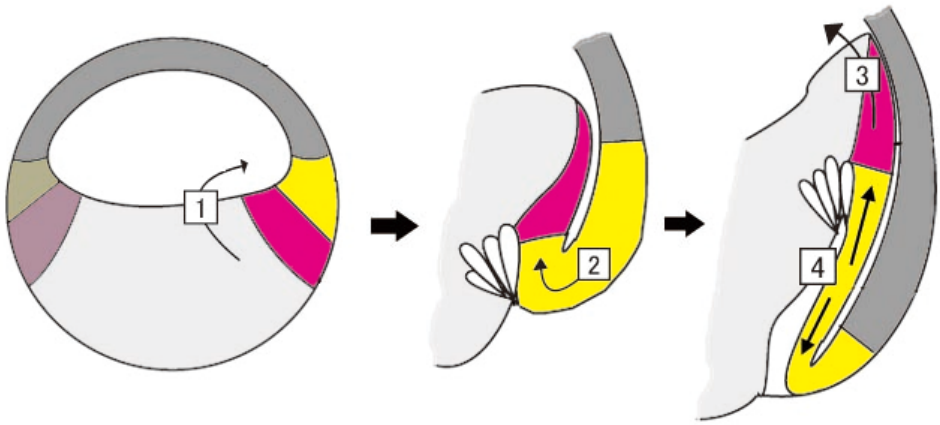

Fig. 1-1 Scheme of dorsal tissue invagination during *Xenopus* gastrulation

At the onset of the gastrulation, the most dorsal region of leading-edge mesoderm (LEM, red) first attach to the inner side of the blastocoel roof (BCR, gray) by vegetal rotation of endoderm (1). After that, the LEM migrates collectively and unidirectionally toward the animal pole (3). On the other hand, the axial mesoderm (AM, yellow) invaginate after the involution of LEM (2), but does not migrate toward the animal pole. In later stage, the AM undergoes convergent extension process to elongate antero-posteror axis (4). In this study, I demonstrated that that whether the physical force is generated by the anterior migration of LEM, and whether such force affects the elongation of AM during gastrulation.

1.4 Approaches of the study

The present study aimed to reveal the magnitude and the role of physical force in the animal development using *Xenopus* gastrulation as a model. As a force generator, I focused on the directional migration of LEM. Then, the study proceeded to characterize the physical force generated by the LEM. In order to measure the force of LEM, the substratum that coats the basal side of the BCR was transferred on a culture dish, and the directional migration of LEM was reproduced on the culture dish. The force was measured based on the extent of displacement of a micro-glass needle with known spring constant which was pushed and bent by the migrating LEM. To further investigate the force transmission between the LEM and surrounding tissues, laser ablation experiments were performed. In this study, I focused on the tensile force on the AM which is connected to the posterior of the LEM and examined whether the force distribution and of AM is affected by the LEM migration. Next, the necessity of the migrating LEM and resulting force was examined in vivo. To prevent the migratory activity of LEM in vivo, fibronectin was depleted by a specific Morpholino oligonucleotide by microinjection in to early embryo. These approaches enabled me to gain new insights into the role of physical force generated by the LEM during *Xenopus* gastrulation.

2. Materials and Methods

2.1 Embryo handling, media, and microinjection

To obtain *Xenopus laevis* embryos, female frogs were injected with 400 units of human chorionic gonadotropin and kept at 17℃ overnight. Male frogs were sacrificed to obtain the testes. *Xenopus laevis* embryos were obtained by standard methods (Morita et al., 2010). Capped mRNAs were injected into the appropriate region of two- or four-cell embryos. The injected embryos were cultured in 3% Ficoll/0.1x Steinberg's Solution (SS) to stage (St.) 9, then placed in 0.3x Marc's Modified Ringer's (MMR) until the appropriate stage. Embryos were staged according to Nieuwkoop and Faber (Nieuwkoop and Faber, 1967).

2.2 mRNA preparation and Morpholino oligonucleotides

Capped mRNAs were synthesized as described previously (Suzuki et al., 2010). *Flag-β-globin* (Suzuki et al., 2010), *Xdd1* (Sokol, 1996), membrane-targeted green fluorescent protein (memGFP) or red fluorescent protein (memRFP) (Morita et al., 2012) were reported previously. Antisense Morpholino oligonucleotides (MOs) specific to *Xenopus* FN were purchased (Gene Tools, Inc). The sequences of xFN1-MO and xFN2-MO were described previously (Davidson et al., 2006). The MOs were mixed (50:50) and injected at 0.35 mM (total injection volume: 10 nl). Standard control-MO (Std.-MO), which does not affect normal *Xenopus* development, was used as a control.

2.3 RT-PCR and in situ hybridization

RT-PCR and *in situ* hybridization were performed as described (Goda et al., 2009). For *in situ* hybridization, the following plasmids were used for probe synthesis: *Xnot-a*

(XL485c16ex, XDB3); *Cerberus* (XL204b07, XDB3); *Xbra* (*Xbra ΔB*, a gift from Ken Cho's laboratory) and *MyoD* (Hopwood et al., 1989). For RT-PCR with dissociated tissues, 10 explants were dissociated from each region at St. 10+. The following primers were used: *Epithelial-keratin I* and *ODC* (Suzuki et al., 2010); *Cerberus* (Yamamoto et al., 2001); and *Xbra* (Shindo et al., 2010).

2.4 Immunohistochemistry

For the immunostaining of FN, embryos were fixed in MEMFA or 3% trichloroacetic acid (Davidson et al., 2004) for 2 hours. Fish gelatin cryosections were prepared and stained as described previously (Suzuki et al., 2010). For dorsal-lip explant staining, the explants were isolated from St. 10 embryos, flattened under a glass-plate bridge, and cultured on non-coated tissue-culture-grade (TC-grade) plastic dishes (CELLSTAR, Greiner) until St. 12.5. The explants were then fixed in MEMFA for 2 hours. To analyze the notochord structure, St. 12.5 embryos were fixed in MEMFA for 2 hours. After fixing, the dorsal region was dissected by razor under a stereomicroscope. Staining was performed as described above. After staining, the embryos were made transparent by replacing the methanol with 2BA:BB (2:1 mixture of benzyl benzoate and benzyl alcohol; also known as Murray's clear solution), and the notochord structure was observed by confocal microscopy (Nikon A1) (see Fig. 3-10A). The following antibodies were used: anti-GFP (1:200; GF200, Nakalai Tesque), anti-RFP (1:300; PM005, MBL), anti-FN (1:300; 4H2, Ramos and DeSimone, 1996), and anti-Flag (1:300; F7425, Sigma). The secondary antibodies were Cy5-conjugated anti-rabbit Cy5 (1:200; Jackson ImmunoResearch), Alexa Fluor 488 anti-mouse

(1:1000; A11017, Molecular Probes), and Alexa 555 anti-rabbit (1:500; A21430, Molecular Probes). Alexa Fluor 546 phalloidin (1:50; A22283, Molecular Probes) was used for actin staining.

2-5 Western blotting of RhoA and Rac1

RhoA activation assay biochem kit (BK036, Cytoskeleton, Inc.) and Rac1 activation assay biochem kit (BK035, Cytoskeleton, Inc.) were used for the quantification of those activities. The dorsal region of embryos at desired stages was excised and lysed in the lysis buffer [50mM Tris pH 7.5, 10mM MgCl2, 0.5M NaCl, and 2% Igepal] with a cocktail of protease inhibitors (contained in the kit). The supernatant of the lysate was sampled and used for the pull-down assay with rhotekin-beads which binds to active RhoA. After that, they were denatured by the same volume of 2x SDS sample buffer [0.5 M Tris-HCl pH 6.8, 10% SDS, 50% glycerin, 5% 2-mercaptoethanol]. After boiling for 5 minutes, the samples were processed in SDS-PAGE, blotted onto the PVDF membrane (Bio-Rad), reacted with the following primary antibodies, and detected using HRP-linked secondary antibodies and ECL Prime kit or ECL Select kit (GE Healthcare). Anti-RhoA polyclonal antibody (RhoA (119), sc-179, Santa Cruz) and anti-Rac1 monoclonal antibody (610651, BD Transduction Laboratories) were used as the primary antibodies.

2.6 Conditioned substratum preparation

The substratum that coats the basal side of the BCR was reproduced in a culture dish as described previously (Nagel et al., 2004; Winklbauer and Nagel, 1991), with minor

modifications (Fig. 2-1). BCR explants were held against the bottom of TC-grade plastic dishes by glass-plates (width 1 mm, thickness No. 1 grade; Matsunami Glass) with glass-plate spacers and silicone grease. After 3 hours of cultivation, the BCR explants were removed by aspiration along with the buffer, and the substrata were saturated with 5% bovine serum albumin (BSA, FractionV, Sigma) in 1x modified Barth's solution (MBS) for 30 minutes. Finally, the solution was replaced with Danilchik's For Amy (DFA) medium (Sater et al., 1993), and this conditioned substrate was used in migration assays and laser ablation experiments. Herein, I call this conditioned substrate "BCR-coating." Given that endogenous positional cues are also reproduced in the dish, the BCR-coating is thought to mimic the BCR on which the mesoderm migrates toward the anterior side. The migration of explants on BCR-coated dishes was observed with an inverted microscope.

2.7 Laser ablation

Explants prepared for live imaging were imaged using an Olympus IX 81 inverted microscope (20× / 0.70 NA dry objective lens, Olympus), equipped with a spinning-disk confocal unit Yokogawa CSUX-1 and iXon3 897 EM-CCD camera (Andor), controlled with Andor IQ2 software. An N_2 Micropoint laser (16 Hz, 365 nm; Photonic Instruments) was focused on the apical surface of an explant to ablate plasma membrane structures. For linear ablations, 16 sequential point ROIs were identified, and an approximately 150-μm incision was cut along them, in the mediolateral direction. Time-lapse images of membrane-localized GFP (mem-GFP) fluorescence were

acquired immediately before, during, and after ablation to measure the displacement of membrane structures. Note that I ablated the outer side of the explants because it is easier to cut stably than the inner side; the ease of ablation may depend on the amount of cell pigmentation (Joshi et al., 2010).

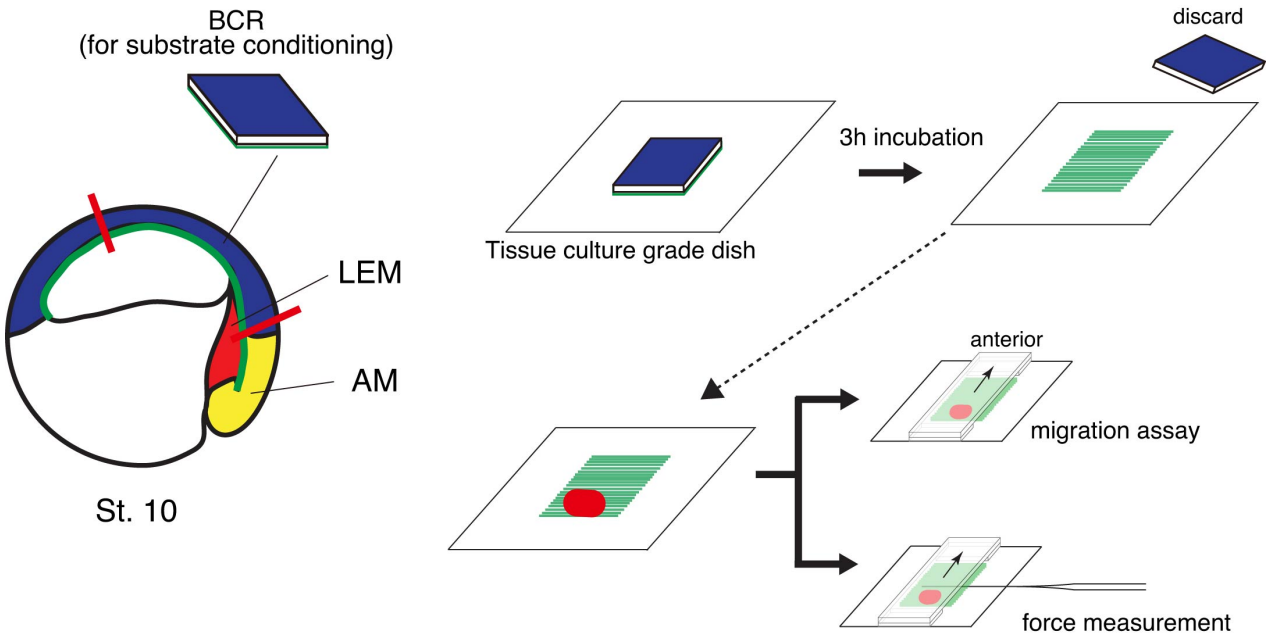

Fig. 2-1 Conditioned substratum preparation

The scheme of substratum conditioning. For details to the text in Materials and Methods. Red lines indicate dissected region. Green lines show fibronectin substrates.

2.8 Force measurement

The force generated by the LEM was measured using a tensile test with a micro-glass needle (see Fig. 3-2A,B). I modified a previously reported technique (Nagayama and Matsumoto, 2008) to fit the force measurement of explant migration. I prepared thin and flexible glass needles and measured the spring constant of the needles prior to the experiments (0.4-0.8 nN/μm). Measurements were done on BCR-coated 35-mm plastic dishes. To place a glass needle in front of a migrating explant, part of the sidewall of the plastic dish was cut off, and a thin layer of grease was applied to the cut edge to keep the culture solution from spilling. The needle was attached to a holder connected to a micromanipulator (MHW-3, Narishige). Images of the needle and explant were acquired by an inverted microscope. Based on the maximum deflection of the glass needle and its spring constant, the maximum force generated by the LEM was estimated using Hooke's law (Equation 1), as follows.

$$F = X_D \times k, \qquad (1)$$

where F is the generated force, X_D is the deflection of the needle tip, and k is the spring constant of the needle.

2.9 Measurement of the shrinkage of dorsal marginal zone (DMZ) tissue

The DMZ of a St. 11.5 embryo was isolated. I immediately separated the involuted- and non-involuted-marginal zones of the explant carefully, and transferred the explant to a non-coated glass-bottom dish. Then I acquired time-lapse images without holding by the glass-plate bridge in DFA for 1 minute, until the beginning of the rounding up of explant. I measured the A-P length of the AM, which was coated with the archenteron

roof, using ImageJ software.

2.10 Image processing, analyses, and statistical analysis

For the migration assay of mesodermal explants, the centroid data were analyzed using "particle analysis," an ImageJ software (Wayne Rasband, National Institutes of Health) function. The obtained data were transferred into Microsoft EXCEL for further quantification. Trace graphs were made by MjoGraph v4.3.1 (http://www.ochiailab.dnj.ynu.ac.jp/mjograph/). The trace lines were merged with acquired images using ImageJ macro. For the force measurements, the needle deflection was measured by ImageJ software using the acquired images. The obtained data were transferred into Microsoft EXCEL and analyzed. To quantify the amount of AM deformation after laser ablation, I used an ImageJ plug-in (PIV, https://sites.google.com/site/qingzongtseng/piv). The parameters were: PIV1=128, SW1=256; PIV2=64, SW2=128; PIV3=32, SW3=64; correlation threshold=0.60. I extracted x and y deformation values from the PIV data, and used them for plot and quantification. In both anterior and posterior side of ablation line, there were little deformation along mediolateral direction (see Fig.3-5A,A'). Thus, I analyzed only y-value in this study. To quantify the morphology of AM cells, Packing Analyzer V2.0 (Aigouy et al., 2010) was used for the segmentation of cells and measurement of the cell aspect ratio. The segmentation data were imported into ImageJ, and the cell angles were quantified. Rose diagrams were drawn by R software (http://www.r-project.org). Statistical analyses, such as the Shapiro-Wilk test and Student's t-test, were done using R software.

3. Results

3.1 Establishment of an in vitro migration assay system of LEM

To investigate the LEM's potential as a force generator, I first reconstructed the directional migratory activity of the LEM at the tissue (explant) level on the culture dish. Previous studies reported that the substrate of BCR that is required for LEM migration could be transferred to culture dishes with necessary information for the directed migration. Thus, I adopted the method with minor modifications (Fig. 2-1, 3-1A; also see Materials and Methods). I prepared the LEM explant by dissection from early-gastrula (St. 10+). The AM explant, which is also the dorsal mesodermal tissue but located at the posterior of the LEM, was also dissected for comparison. The LEM and AM explants of approximately equal size (approx. 500 x 500 μm) were placed on BCR-coated dishes with glass-plate bridges, and the direction and velocity of the collective cell movement were determined. The isolation of the LEM and AM tissues by dissection was confirmed by RT-PCR for several markers (Fig. 3-1B). *Cerberus*, a LEM marker, and *Xbra*, an AM marker, were highly expressed in the LEM and AM explants, respectively, with negligible cross-contamination, indicating that each region was isolated from the embryo properly.

During culture, the LEM migrated unidirectionally on the substrate, toward the original anterior side of the BCR (Fig. 3-1C,D). In contrast, the AM showed a wandering movement around its initial position, and no significant directed migration was observed (Fig. 3-1C, D). The mean velocity along the A-P direction of the LEM was 1.46±0.48 and that of the AM was 0.05±0.52 μm/minute (LEM n=20, AM n=15, mean±s.d.; from 0 to 180 minutes). In later phases of the culture, the AM explant elongated but did not migrate (Fig. 3-1C). These results showed that the LEM can

migrate actively toward the anterior side while the AM has little migratory capacity on the BCR substrate. This tendency is consistent with previous reports showing that LEM and AM cells have different migratory activities (Kwan and Kirschner, 2003; Wacker et al., 1998; Winklbauer, 1990). Although a direct comparison is not possible, the velocity of migrating LEM is not greatly different with the velocity of the mesendodermal mantle closure reported previously (Davidson et al., 2002). From these observations, I concluded that LEM and AM have different migratory capacity in vivo and that this assay system reflects endogenous migratory activities of *Xenopus* mesodermal tissues in gastrula and thus it is suitable for force measurement of LEM.

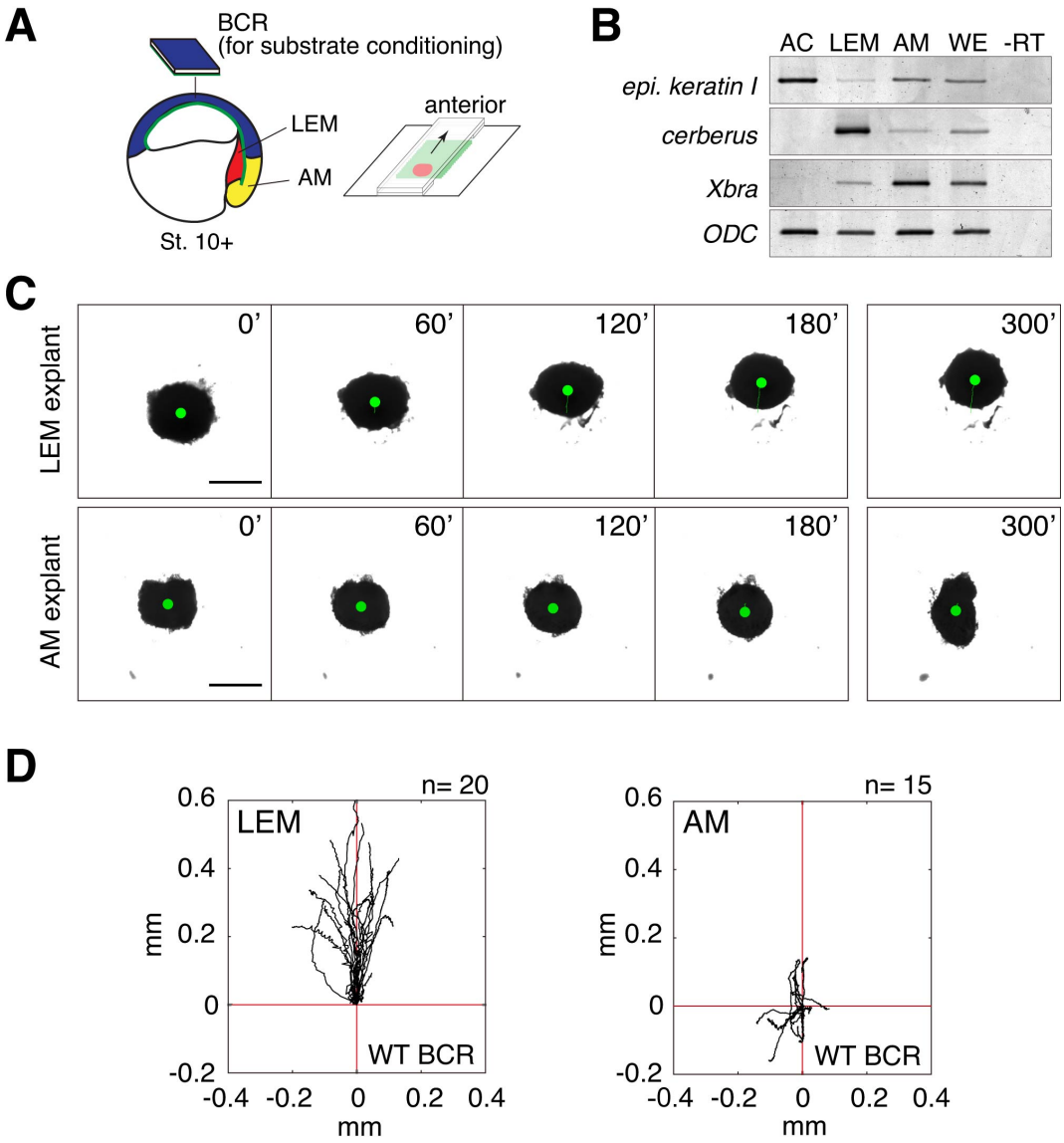

Fig. 3-1 In vitro migration of the LEM and AM

(A) Scheme of the *in vitro* migration assay. The BCR, LEM, and AM were dissected from St. 10+ embryos. The BCR was used for substrate conditioning. Green lines on the BCR indicate the fibronectin layer.

(B) RT-PCR confirmation of the dissected animal cap (AC), LEM, and AM. *Epidermal keratin I* (*epi. keratin I)*, epidermal marker; *Cerberus*, LEM marker; *Xbra*, AM marker; *Ornithine decarboxylase (ODC)*, internal control. WE, whole embryos; –RT, control experiment without reverse transcriptase.

(C) Still images from a time-lapse movie of LEM and AM on a normal BCR-coated dish. Green filled circles indicate the centroid of the explant. Green lines are traced lines. The animal pole on the reproduced substrate is up. Scale bars: 500 μm.

(D) Tracings of LEM (left) and AM (right) centroids migrating on a BCR-coated dish. Black lines show individual traces for 5 hours. Crossed red lines indicate the initial point. In both experiments, wild type-BCR explants were used for the BCR coating.

3.2 Force measurement of LEM migration

To determine the amplitude of the force generated by the migrating LEM, I measured its absolute value using a micro-glass needle whose stiffness/spring constant had been pre-determined (Fig. 3-2A,B). As the LEM migrated anteriorly on the BCR-coated dish, the deflection of the needle increased (Fig. 3-2C). The migrating LEM was stopped by the bent needle at the point where the force generated by the LEM reached a peak (Fig. 3-2D). By measuring the deflection of the needle, the mean force generated by a single LEM explant (approx. 500 x 500 μm) was calculated to be approximately 40 nN (n=14, 41.1±11.5 nN, mean±s.d., Fig. 3-2E). When explants of different sizes were cut, the force magnitude also varied; smaller explants generated less force and larger explants generated greater force (Fig. 3-3A). This result indicates that the magnitude of tissue-generated forces increases in a tissue-size (cell-number) dependent manner. Interestingly, the value of Force/Area showed opposite distribution; it decreased in a tissue-size dependent manner (Fig. 3-3B). Together, these findings directly demonstrated that the migrating LEM indeed acts as a considerable force generator during gastrulation, and also showed that the relationship between tissue-size and generated force in the LEM.

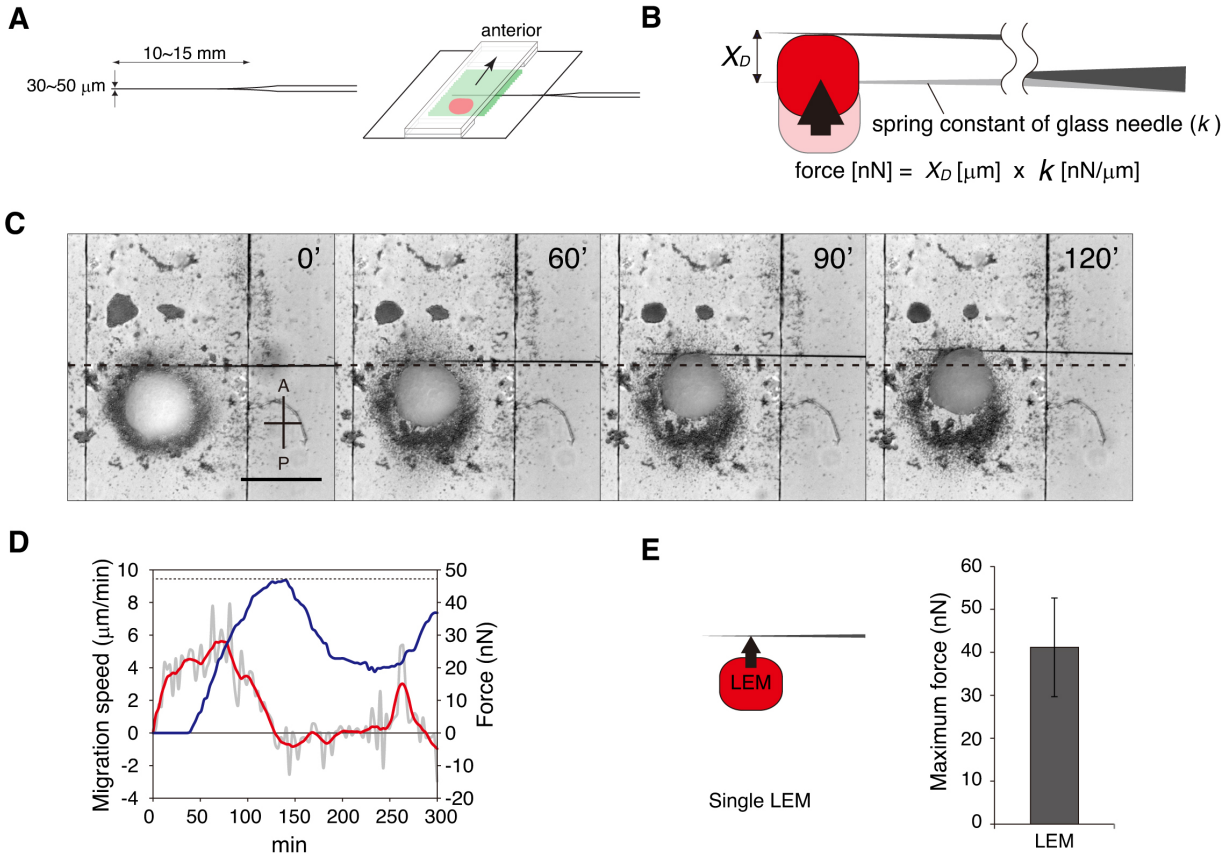

Fig. 3-2 Force measurement with a glass needle

(A) The size of the micro-glass needle and set-up of the experiment are shown at the left and right, respectively. Red filled circle represents the LEM explant. Green lines on the dish indicate the conditioned substrate.

(B) Schematic of the experimental strategy for force measurement with a micro-glass needle. The generated force was calculated as described in Materials and Methods.

(C) Still images from a time-lapse movie of the force-measurement experiment (Movie S2). Black dotted line indicates the initial position of the micro-glass needle. Anterior of the BCR-substrate is up. Scale bar: 500 μm.

(D) An example of the relationship between generated force and migration speed. Red line shows the moving average migration speed. Blue line indicates generated force. Gray line is the original migration-speed data. Black dotted line indicates the maximum generated force.

(E) Schematic of prepared explants and measured maximum force obtained from LEM (n=14, 41.1±11.5 nN, mean±s.d.). Single LEM explants were cut into pieces of about 500 x 500 μm.

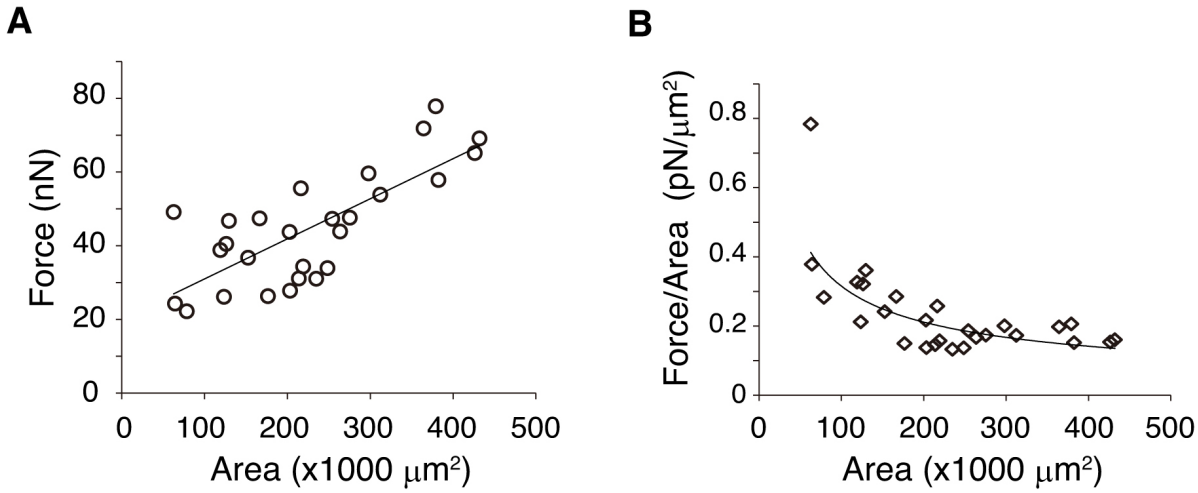

Fig. 3-3 Force measurement with various size of the LEM
(A) Quantification of the maximum force obtained with LEM explants of different sizes (n=27). Circles indicate individual samples. The best-fit line is shown ($R^2 = 0.57$).
(B) Quantification of the Force/Area value obtained with LEM explants of different sizes (the same data set as Fig. 3-3A). The best-fit curve is shown ($R^2 = 0.58$).

3.3 LEM migration exerts pulling force on the AM

Next, I considered whether this physical force influences the force distribution of neighbor tissues. Here, I focused on the AM. The AM undergoes convergent extension (CE) movement, that is known as a key process of body axis elongation during gastrulation (Keller et al., 2000). However, before the AM shows active elongation, the AM does not shows directional migration toward the animal pole while the LEM actively migrates anteriorly (Fig. 3-1C). Therefore, there was the possibility that the LEM pulls the AM along A-P direction by its directional migration at least until AM elongation driven by CE occurs.

To test whether the AM receives a force generated by the actively migrating LEM, I performed laser ablation experiments; laser ablation is an excellent method for estimating the force distribution in tissues undergoing morphogenesis (Kiehart et al., 2000; Martin et al., 2010; Morita et al., 2012). Explants of mem-GFP-expressing DMZ were dissected from St. 10+ embryos and flattened under glass-plates onto a piece of a BCR-coated dish. The adherent explant was turned upside down into a culture dish, and images from the outside of the explant were acquired by inverted microscopy (Fig. 3-4A). In this experiment, I prepared two types of explants: one containing migratory LEM, and one lacking it (Fig. 3-4B). After a 2-hour incubation, which is sufficient for forward migration of LEM but well before AM elongation, I ablated a mediolaterally aligned group of AM cells that were several cell diameters posterior to the LEM/AM boundary. Immediately after the laser ablation (Δ=4 seconds) of the AM with LEM, I observed the cutting edges to be displaced in the anterior and posterior directions (Fig. 3-4C,C') but with no significant mediolateral displacement (Fig. 3-5A,A'). Particle

image velocimetry (PIV) analysis, performed to quantify the magnitude of the displacement, showed a high deformation field in the AM with LEM (Fig. 3-4E). In contrast, I observed smaller recoils in the cutting edges of the AM that lacked LEM (Fig. 3-4D,D',F). I measured the mean displacement of the regions anterior and posterior to the ablation line (Fig. 3-4E,F; white boxed regions), and found a significant difference in the recoil between the AM with and without LEM (Fig. 3-4G), suggesting that tension is applied on the AM along the A-P axis with the presence of LEM. These results demonstrate that LEM indeed exerts pulling forces, and that such forces transmitted to the AM could have affected the force distribution of the AM along A-P direction.

I also measured the force generated in explants in which the connections between the LEM, AM, and ectoderm were maintained (LAE explants). The magnitude of the LEM-generated force in the LAE explants was smaller than in the LEM-only explants (n=9, 25.1±12.3 nN, mean±s.d., Fig. 3-5D,E). For this, I measured the force prior to the AM elongation occurs, suggesting that the AM and ectoderm did not contribute to the force generation, but rather consumed the force while LEM migrated in the A-P direction at this stage. I propose here that LEM has an ability to pull the AM along the A-P direction with their anterior migration, like a power car with an engine pulls passenger cars.

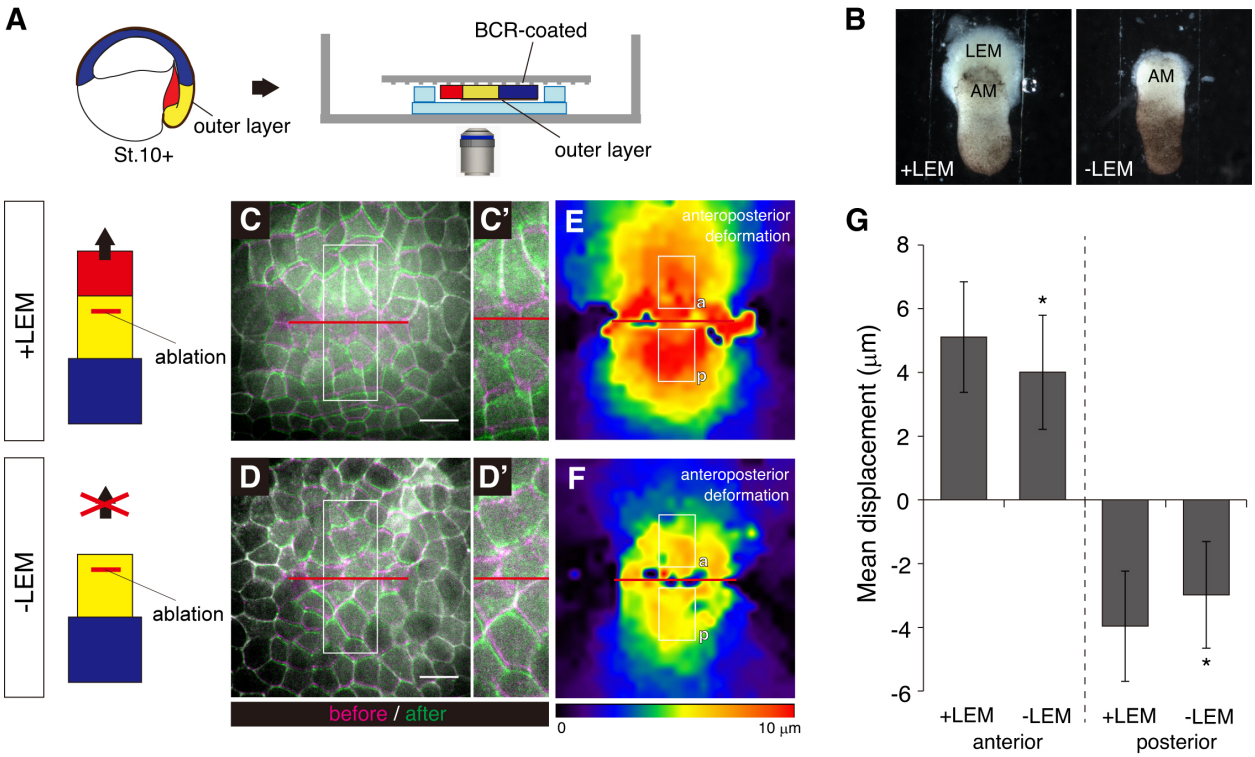

Fig. 3-4 AM receives tension from LEM.

(A) Schematic of the laser ablation experiment. DMZ was cut from a St. 10+ embryo and flattened on a piece of a BCR-coated dish. The explant, held by glass-plates, was then turned upside-down on a culture dish. Brown line indicates the epidermis layer. White dashed line indicates BCR-coating.

(B) Bright-field images of explants after a 2-hour incubation. Two types of explants were prepared: one included migratory LEM (+LEM) and the other did not (-LEM).

(C-D') Laser ablation experiment in the presence (C) and absence (D) of LEM. AM was ablated along the mediolateral axis (red lines). Fluorescent images of mem-GFP-injected explants were taken just before (magenta) and immediately after (Δt = 4 seconds, green) ablation. White boxed region in C and D is magnified in C' and D', respectively. Scale bar: 50μm.

(E and F) Deformation map generated by PIV analysis showing the magnitude of A-P directed displacement. Lower displacements are indicated with the color range of purple to blue; regions of high traction are in the color ranges of yellow to red. White-boxed regions indicate the ROIs for quantification. a, anterior. p, posterior.

(G) Mean displacements calculated from the white-boxed regions in E and F. Positive and negative values of vertical axis indicate anteriorly deformation and posteriorly deformation, respectively. +LEM explants generated greater recoils on the anterior and posterior side (n=26, 7 batches, 5.11±1.73 μm (anterior), 3.96±1.73 μm (posterior), mean±s.d.) of the ablation line compared with the –LEM explants (n=27, 7 batches, 4.00±1.79 μm (anterior), 2.98±1.67 μm (posterior), mean±s.d.). *P<0.05.

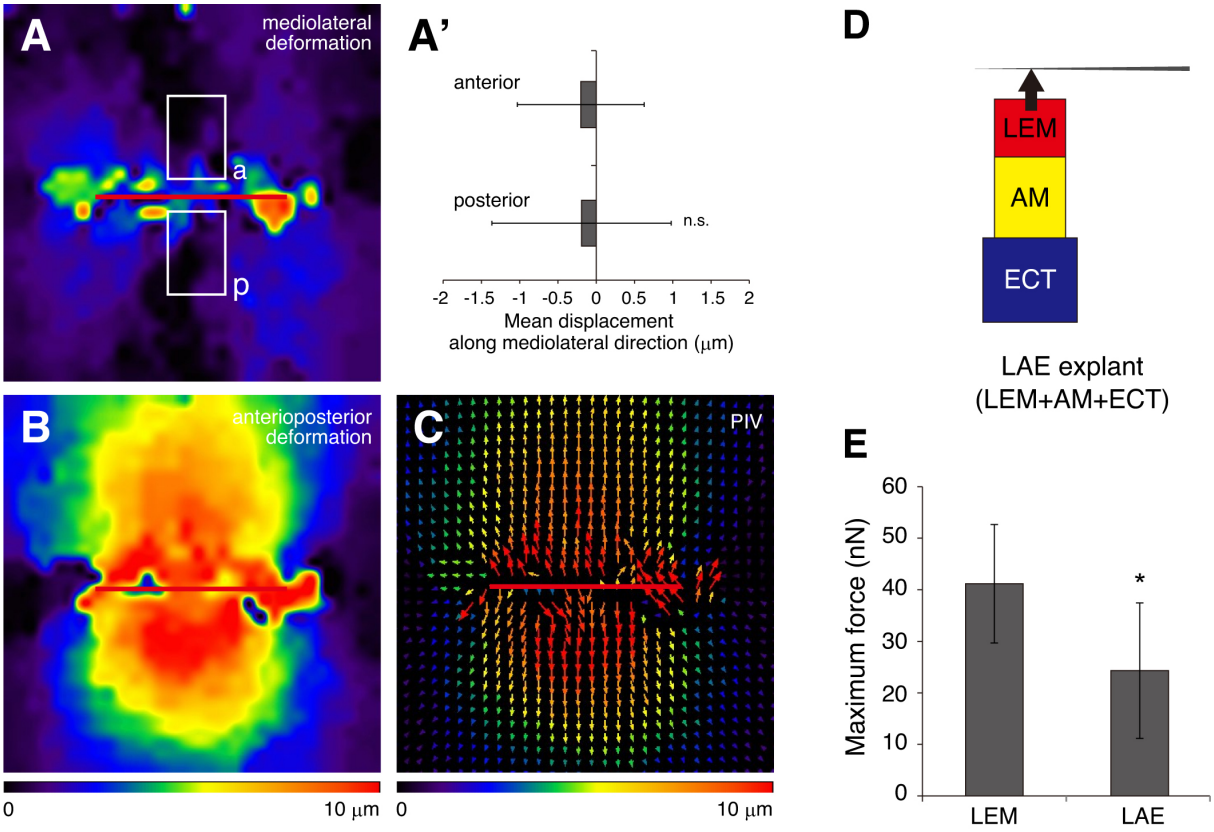

Fig. 3-5 Supplementary of laser ablation experiments and force measurement.
For the analysis for mediolateral displacement after laser ablation, the same data set as Fig. 3-4C, C', and E were analyzed for mediolaterally directed displacement.
(A) Deformation map generated by PIV analysis showing the magnitude of mediolaterally directed displacement. White-boxed regions indicate the ROIs for quantification. a, anterior. p, posterior.
(A') Mean displacements calculated from the white-boxed regions in A. Positive and negative values of horizontal axis indicate mediolateral deformation. In both anterior (n=26, 7 batches, -0.20±0.83 μm, mean±s.d.) and posterior side (n=26, 7 batches, -0.19±1.17 μm, mean±s.d.) of ablation line, little deformation along mediolateral direction was observed. Moreover, there was no significant difference between anterior and posterior.
(B) Deformation map generated by PIV analysis showing the magnitude of A-P directed displacement (identical to Fig. 3-4E).
(C) Vector plot generated by PIV analysis. This data include both A-P and mediolateral deformation.
In these figures, red lines indicate ablation line. Lower displacements are indicated with the color range of purple to blue; regions of high traction are within the color ranges of yellow to red.
(D) Schematic of prepared explants. LAE explants were prepared as in Fig. 3-4.
(E) Measured maximum force obtained from LEM (the same data set as Fig. 3-2E) and LAE explants (n=9, 25.1±12.3 nN, mean±s.d.). Error bars represent s.d. *P<0.05.

3.4 The migrating LEM is required for normal gastrulation movement and proper notochord formation.

To address whether the pulling force generated by LEM functions in the morphogenesis of the *Xenopus* AM, I knocked down fibronectin (FN) in the BCR, to non-destructively inhibit the migratory activity of the LEM and thereby reduce the force on the AM. In the *Xenopus* embryo, FN is expressed on the basal surface of BCR cells; the LEM migrates toward the animal pole on this substrate, in contact with the FN fibrils (Boucaut and Darribere, 1983; Davidson et al., 2002; Lee et al., 1984; Winklbauer and Keller, 1996; Winklbauer and Nagel, 1991). Thus, I injected xFN-MO into the ventro-animal pole of 2-cell-stage embryos just before the beginning of the second cleavage (Fig. 3-6A). Under this injection condition, the xFN-MO decreased FN exclusively in the BCR region (Fig. 3-6B) and not in the dorsal mesoderm, so that only the interaction between the BCR and LEM should be inhibited. I confirmed the specificity of the xFN-MO effect by comparing the expression of FN in dorsal-lip explants from control (Std.)-MO- or xFN-MO-injected embryos, and found that the FN expression was not impaired by BCR-targeted MO injections (Fig. 3-6C,D,F). In contrast, xFN-MO injection at the 4-cell stage, targeted to the DMZ, markedly decreased FN expression in dorsal-lip explants (Fig. 3-6E,F). These results confirmed that the exclusion of unwanted effects of the BCR-targeted xFN-MO knockdown on the AM region was achieved, although the interpretation of the xFN-MO effects may be more complicated considering the broad function of FN on tissue architecture. However, BCR structure was almost normal in the BCR-FN morphants (Fig. 3-6B), and the examination of the dorsal patterning in the BCR-FN morphants revealed no obvious

changes in the expression of marker genes tested (Fig. 3-7), suggesting that BCR-FN MO did not affect tissue architecture and cell differentiation. Thus, I concluded that the major defect of BCR-targeted injection of xFN-MO is the reduction of the LEM migration activity.

When I used the xFN-MO-injected BCR (MO-BCR) for the conditioned substrate, the anterior migration of LEM was significantly inhibited (Fig. 3-8). Laser ablation experiments also revealed that the LEM reduced the tension in the AM on the MO-BCR coating (Fig. 3-9A-C). Furthermore, I investigated whether the tension on the AM changed in the *in vivo* situation. According to previous reports (Matsumoto et al., 2004), tissues that are under passive tension shrink due to the release of residual stress after their isolation from neighboring tissues. Thus, I observed the deformation of DMZ tissue immediately after its isolation from St. 11.5 embryos, by measuring the length of the AM in these explants (Fig. 3-9D; see Materials and Methods). The isolated tissue from control embryos showed constant shrinking, indicating that the AM is under tension at this stage. Notably, the isolated tissues from embryos in which the xFN-MO was targeted to the BCR (BCR-FN morphants) shrank more slowly (Fig. 3-9E-F). In this assay, there is the possibility that I missed the very first exponential deformation. However, these data still indicated the difference between the control and BCR-FN morphants, suggesting that MO-BCR indeed reduced the tension in the AM by inhibiting LEM migratory activity.

Control embryos in which Std.-MO was targeted to the BCR underwent normal gastrulation (Fig. 3-10A,E). In contrast, the BCR-FN morphants showed a higher frequency of gastrulation defects (Fig. 3-10B,E). I also analyzed the notochord structure

in BCR-injected embryos by *in situ* hybridization of *Xnot*, a notochord marker. Control embryos showed a well-converged and elongated labeled domain, indicating that their notochord formed normally (Fig. 3-10C,F). The *Xnot*-expressing region of the BCR-FN morphants was wider and shorter than that of the controls (Fig. 3-10D,F). At a later stage, the BCR-FN morphants closed their blastopore, but their A-P length was reduced compared with controls (Fig. 3-10G,H). These results suggest that the anterior migration of LEM and the resulting strain may have important functions in the control of CE of the AM, but through unknown processes.

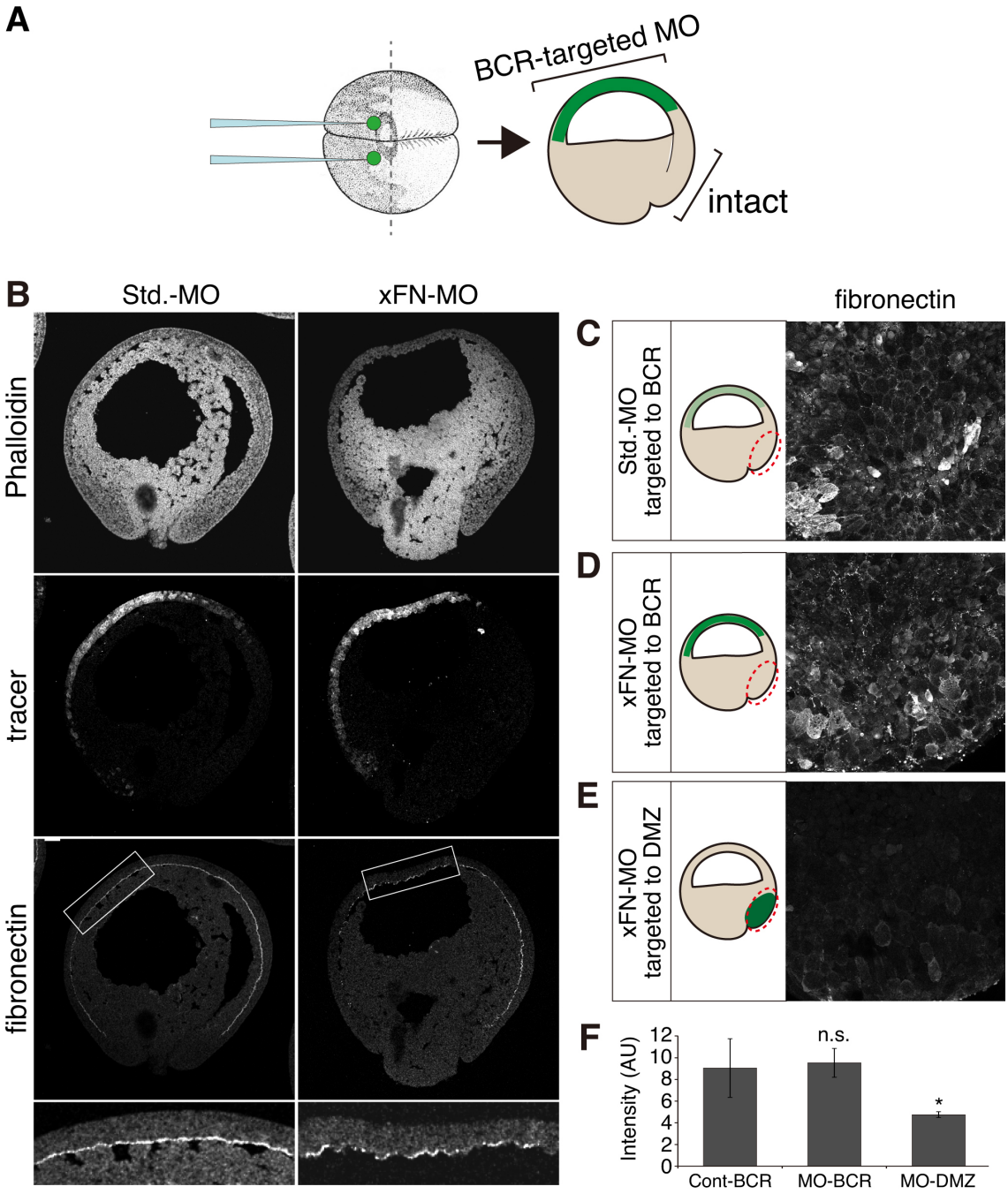

Fig. 3-6 BCR-targeted xFN-MO injection only affects the BCR region.
(A) Schematic of BCR-targeted MO injection. At the beginning of the 4-cell stage, 10 nl of MOs was injected into the ventro-animal pole of both blastomeres (green) at 0.35 mM.
(B) Immunostaining of actin, flag-β-globin (tracer), and fibronectin (FN) in BCR-targeted MO-injected embryos. White boxed regions in the FN-stained images are magnified at the bottom. Dorsal is to the right.
(C-E) Scheme of experiments and FN immunostaining images in dorsal-lip explants. C, Std.-MO targeted to BCR; D, xFN-MO targeted to BCR; E, xFN-MO targeted to DMZ. Green indicates the MO-expression site and red dotted lines indicate explanted region.
(F) Quantification of the mean intensity of FN in dorsal lip explants. Results for Std.-MO injection targeted to the BCR (Cont-BCR), at the left (n=6); xFN-MO targeted to BCR (MO-BCR), in the middle (n=4); and xFN-MO targeted to the DMZ (MO-DMZ) at the right (n=3). Error bars indicate s.d. *P<0.05.

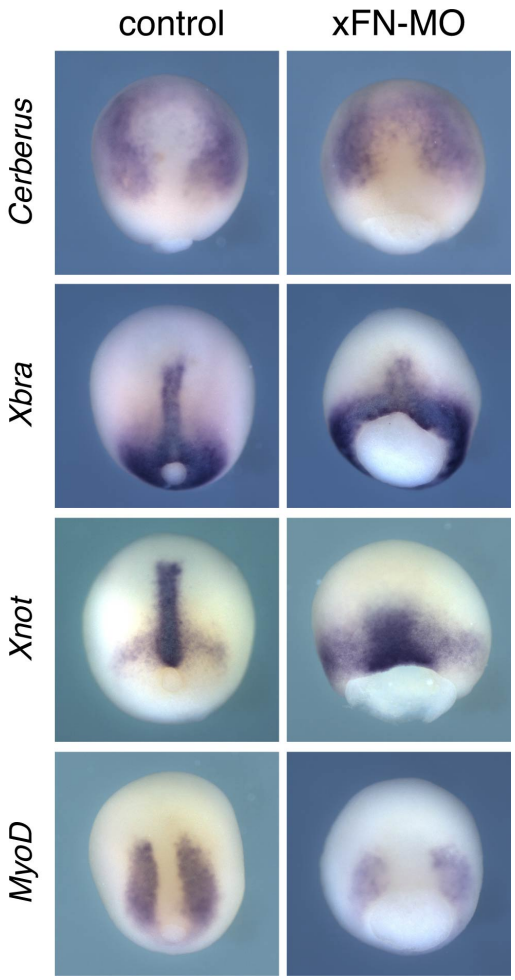

Fig. 3-7 No effect of xFN-MO injection into the BCR on patterning of the dorsal region
In situ hybridization analysis of control and BCR-FN morphants. *Cerberus* is dorsoanterior mesendoderm marker. *Xbra* is a pan-mesoderm marker. *Xnot* is a notochord marker. *MyoD* is a somite maker. Although the notochord structure was shortened, the dorsal patterning was not affected by the BCR-targeted xFN-MO injection.

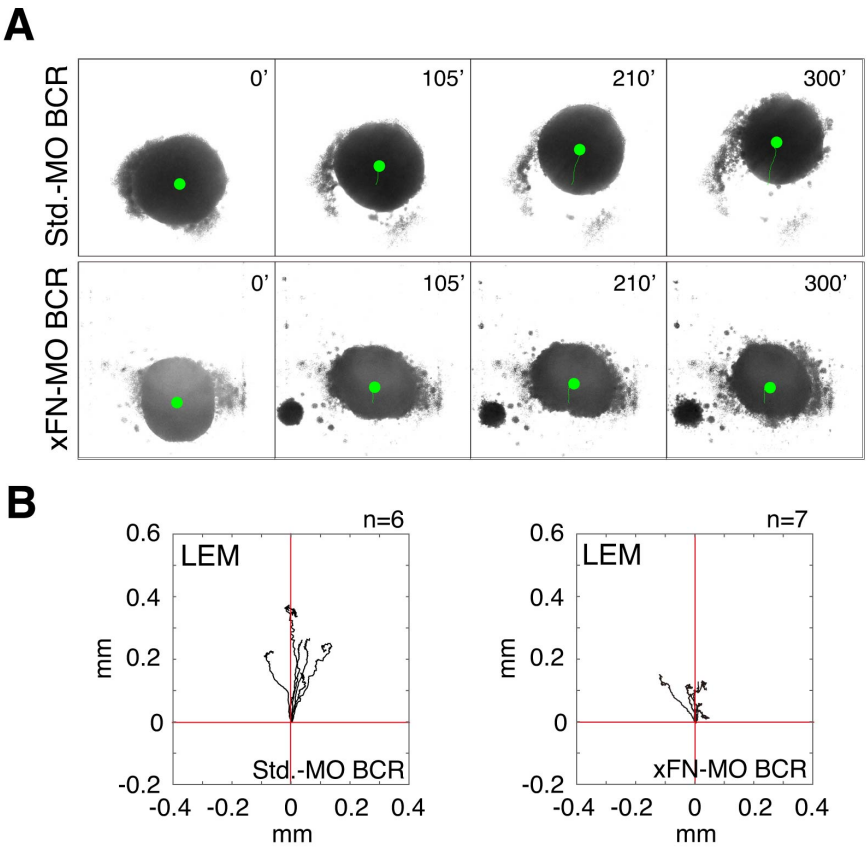

Fig. 3-8 Significant inhibition of LEM's anterior migration on xFN-MO-injected BCR.

(A) Still images from a time-lapse movie of LEM on BCR coating from Std.-MO-injected embryos (upper) or xFN-MO-injected embryos (bottom). Green filled circles indicate the explant centroid. Green lines trace the movement of the centroid. The anterior of the reproduced substrate is up.

(B) Traces of LEM centroid migratory path on BCR coating from Std.-MO-injected embryos (left, *n*= 6) or xFN-MO-injected embryos (right, *n*= 7). Black lines show individual traces obtained for 5 hours. The intersection of the red lines indicates the initial point. The animal pole of the reproduced substrate is up. In both experiments, wild-type LEM explants were used.

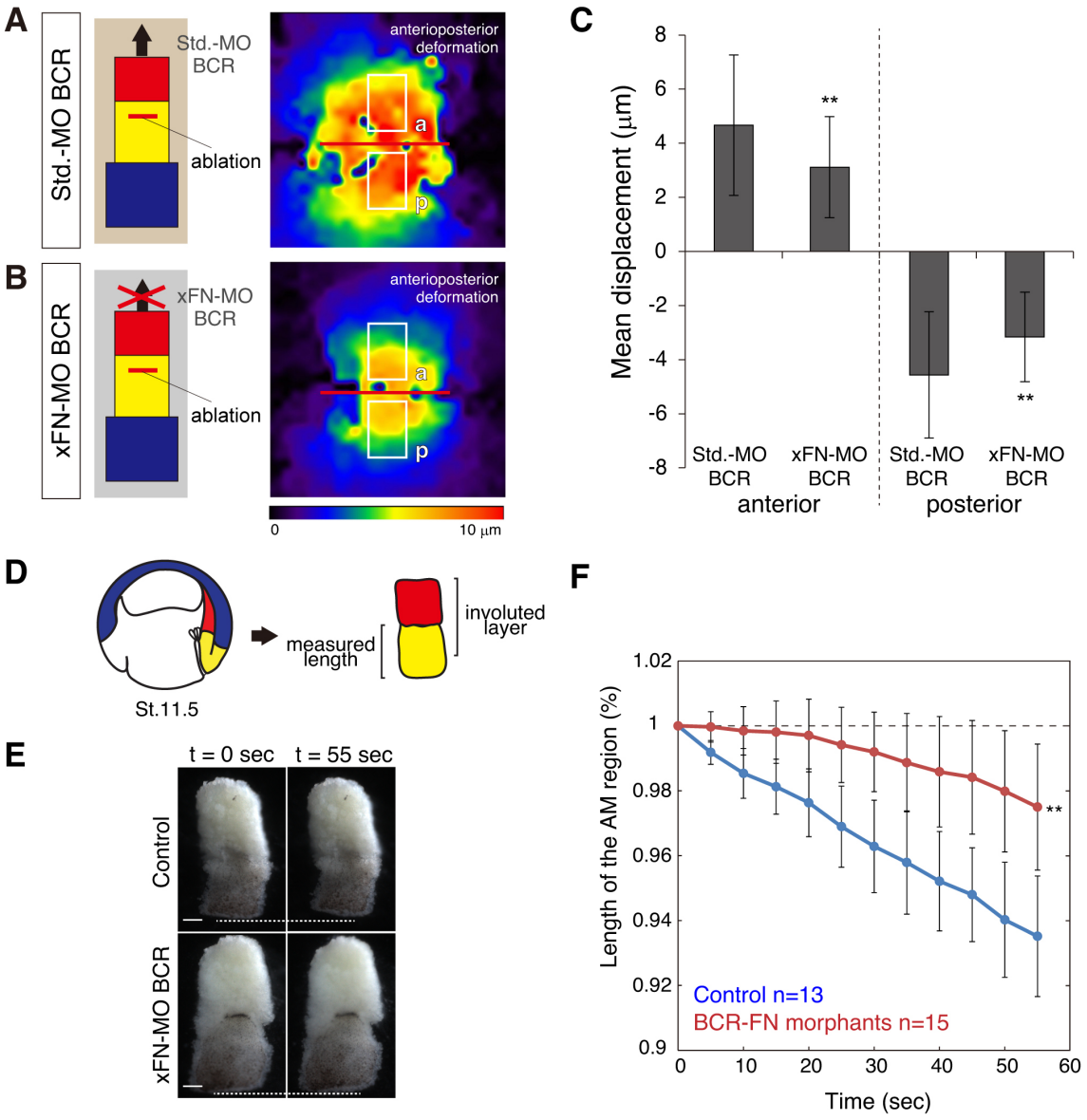

Fig. 3-9 Reduction of the LEM-generated pulling force by BCR-targeted xFN-MO injection

(A and B) Scheme of experiments and deformation map generated by PIV analysis showing the magnitude of A-P directed displacement. Explants were prepared as shows in Fig. 3-4. (A) Explants were plated on the Std.-MO BCR. (B) Explants plated on the xFN-MO BCR. Red lines indicate ablation lines. White boxed regions indicate the ROIs for quantification. a, anterior. p, posterior.

(C) The mean displacements along A-P direction calculated from the white boxed regions in A and B. Explants on the control BCR-coating showed significantly greater recoils (n=50, 12 batches, 4.67±2.59 μm (anterior), 4.56±2.34 μm (posterior), mean±s.d.) than explants on the xFN-MO BCR-coating (n=38, 9 batches, 3.11±1.87 μm (anterior), 3.16±1.66 μm (posterior), mean±s.d.). $^{**}P<0.01$

(D) Scheme of the DMZ shrinkage assay. See Materials and Methods for details.

(E) Bright-field views of the DMZ in the shrinkage assay. White dotted lines indicate the initial position of the edge. Scale bars: 200 μm.

(F) Length of the AM during shrinking. Blue indicates control (n=13), red indicates BCR-FN morphants (n=15). Error bars indicate s.d. $^{**}P<0.01$.

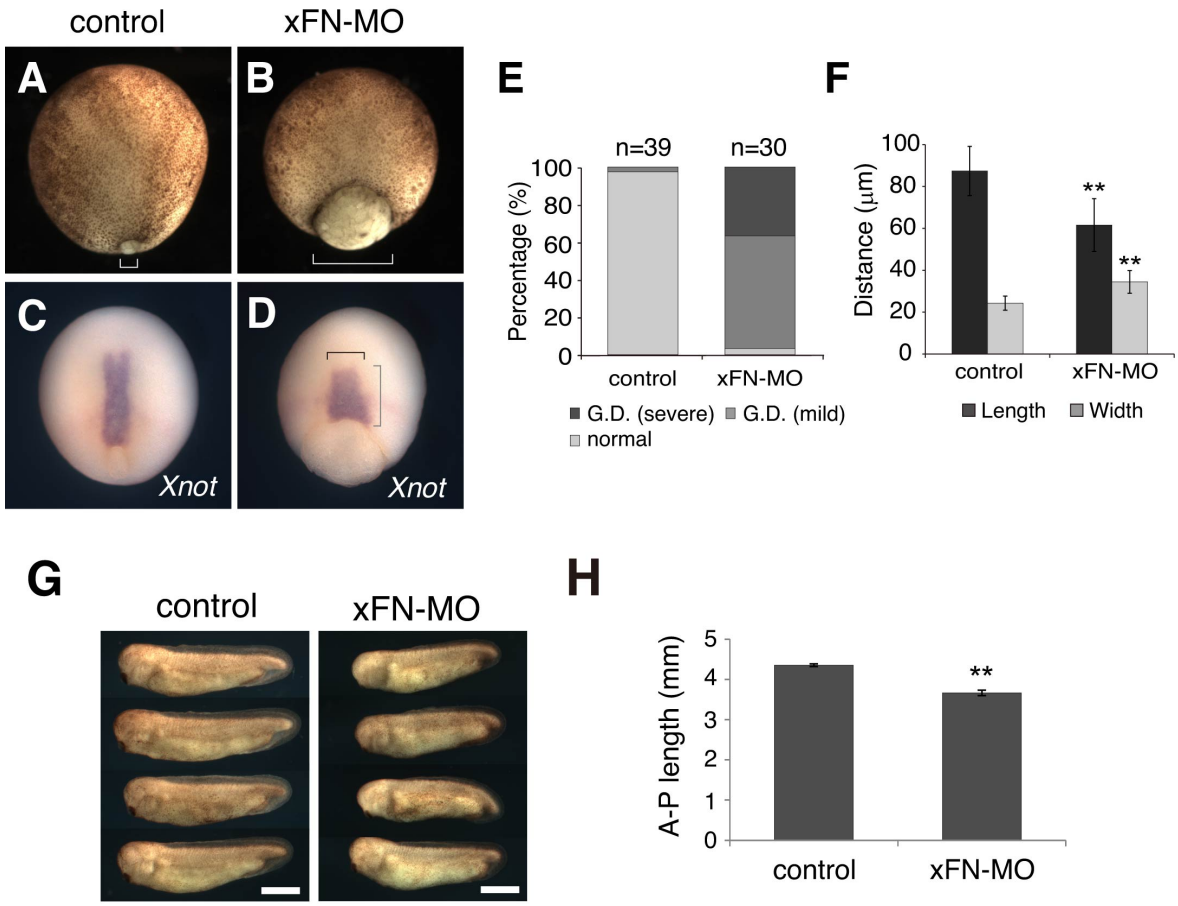

Fig. 3-10 Migrating LEM is necessary for normal gastrulation movement and elongation of AM.

(A-B) Dorsal views of BCR-injected morphants at St. 12.5. The white brackets indicate the diameter of the blastopore.

(C-D) Expression of *Xnot*, an AM marker, in a Std.-MO (control) (C) or xFN-MO (D) -injected embryo. The black and gray brackets in (D) indicate the widened and shortened notochord.

(E) Quantification of embryos showing gastrulation defects (G.D.). Almost all control embryos were normal (n=39), whereas the BCR-FN morphants (n=30) showed a higher frequency of G.D. If the size of the yolk plug was bigger than a third of the diameter of the embryo, I categorized the sample as severely defective.

(F) Quantification of the length and width of *Xnot* staining. Compared with controls (n=8), the xFN-MO-injected embryos (n=7) showed a widened and shortened notochord. Error bars indicate s.d. $^{**}P<0.01$.

(G) Morphants at a late stage (St. 31). Scale bar: 1 mm.

(H) Quantification of the A-P length of the late morphants. The dorsal axis extension was moderately reduced in the xFN-MO-injected embryos (n=31), while the Std.-MO-injected embryos (n=21) were normal. Error bars indicate s.d. $^{**}P<0.01$

3.5 Cell elongation and orientation are disrupted in AM lacking migrating LEM

I next analyzed the defects of the notochord formation at the cellular level in BCR-FN morphant embryos, retaining the *in vivo* structure as much as possible (Fig. 3-11A; also see Materials and Methods). In control embryos, the AM exhibited clear notochord–somite boundaries (Fig. 3-11B, yellow dotted lines), and the AM cells were well aligned in the mediolateral direction; in addition, most AM cells had a high aspect ratio, and formed the typical interdigitized arrangement (Fig. 3-11C,D). In contrast, the AM cells in BCR-FN morphants did not form clear boundaries (Fig. 3-11B', yellow dotted lines). These cells did not elongate, and the alignment angles along the mediolateral direction were also perturbed, resulting in the failure of convergence (Fig. 3-11C',D'). These results indicate that the notochord malformation in embryos with reduced LEM motility is due to the misorientation and aborted elongation of the cells.

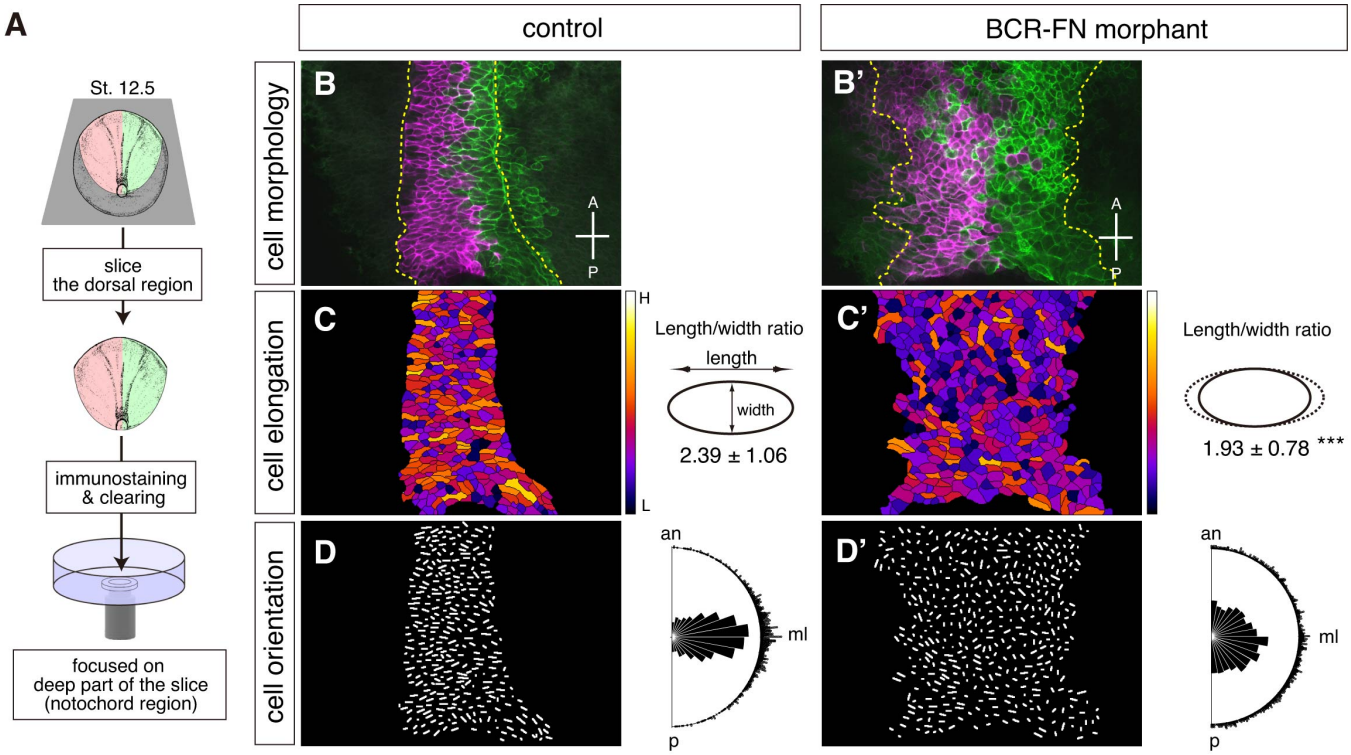

Fig.3-11 Cell orientation and elongation in the AM were disrupted by the reduction of LEM migratory activity

(A) Scheme of notochord imaging. Gray square shows the plane of section. Membrane-localized RFP and GFP were each injected into one side of the embryo.

(B-D') Confocal image and analysis of control embryos (B-D) and BCR-FN morphants (B'-D') at St. 12.5.

(B and B') AM cells expressing mem-RFP/mem-GFP within a confocal section. Yellow dotted lines indicate the notochord-somite boundaries.

(C and C') Cell aspect ratio (AR) analysis. Yellow and orange indicate high AR cells; blue and purple indicate low AR cells. The mean AR in the controls (C) was 2.39±1.06 (n=843 cells from 3 embryos, mean±s.d.); in the morphants (C'), the mean AR was 1.93±0.78 (n=1042 cells from 3 embryos, mean±s.d.). Dotted line indicates the mean AR of controls. ***P<0.005.

(D and D') Analysis of cell long-axis angle. Sample numbers were the same as in C and C', respectively. Rose diagrams show the frequency distribution of the cells' angles in D and D'. Dots along the outer periphery indicate individual cell angles. an, anterior; ml, mediolateral; p, posterior. Anterior of the embryos is up.

3.6 *RhoA and Rac1 activity at the AM did not change in BCR-FN morphants*

Because it has been shown that small GTPases RhoA and Rac1, activated by Dishevelled of the Wnt/PCP signal, are important for cell polarity formation and motility of AM cells during CE (Berger et al., 2009; Habas et al., 2003; Habas et al., 2001; Tada et al., 2002; Tahinci and Symes, 2003; Wallingford et al., 2000), I examined the activities of those proteins in the AM in BCR-FN morphants. To examine the RhoA and Rac1 activity in AM, dorsal regions which did not contain xFN-MO-injected BCR regions were isolated at St. 12.5 (Fig. 3-12A), and used in the pull-down assay with pull-down beads which bind specifically to the GTP-bound form of RhoA and Rac1, respectively. As a result, there was no difference of the dorsal RhoA and Rac1 activity between control embryos and BCR-FN morphants (Fig. 3-12B). These results indicate that the disruption of anterior migration of LEM did not affect RhoA and Rac1 activity in the AM, suggesting that Wnt/PCP pathway in the AM might be unaffected even if the cell elongation and alignment were perturbed. Moreover, these results also suggest that LEM controls notochord formation through a Wnt/PCP-independent mechanism.

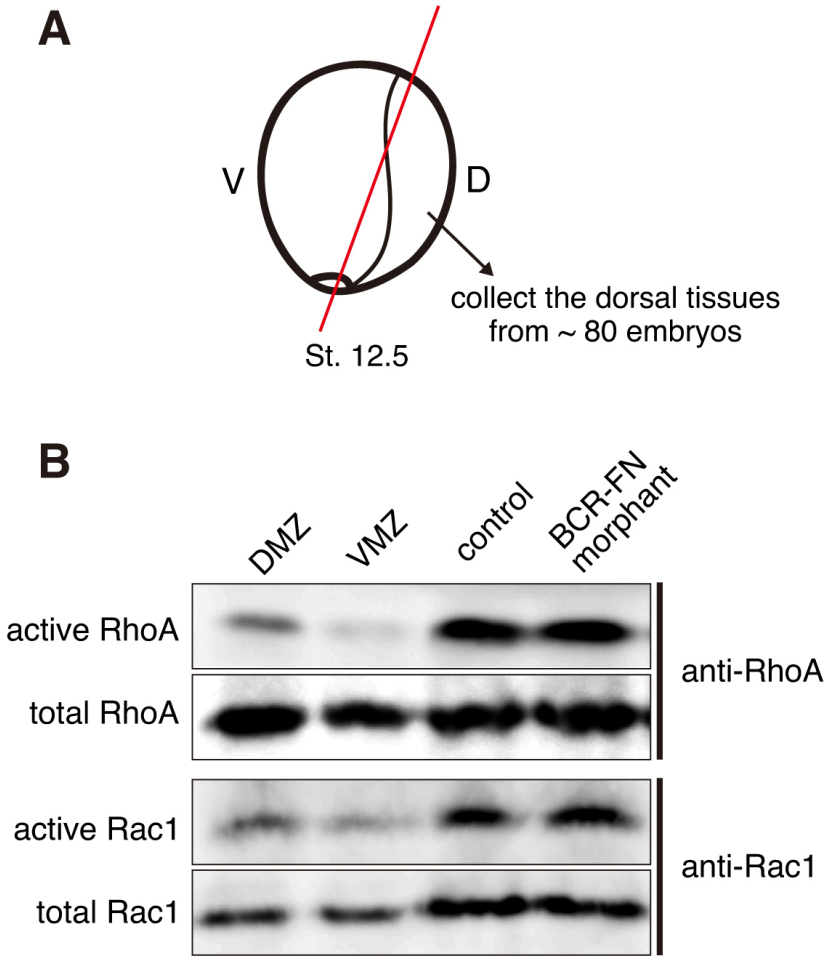

Fig. 3-12 Knockdown of LEM's anterior migration did not decrease dorsal RhoA and Rac1 activity.
(A) Scheme of tissue dissection for western blot analysis. Dorsal regions which did not contain MO-injected BCR regions were isolated at St. 12.5
(B) The dorsal activities of RhoA and Rac1 were not changed in BCR-FN morphants. DMZ explants and ventral marginal zone (VMZ) explants were dissected from St. 10.5 embryos and used for control; RhoA and Rac1 were highly activated in DMZ, but not in VMZ.

3.7 Anterior migration of the LEM cooperates with the Wnt/PCP pathway to establish the notochord

It has been shown that Wnt/PCP signaling plays a critical role in CE movement in the *Xenopus* gastrula (Tada et al., 2002; Tada and Heisenberg, 2012; Wallingford et al., 2002). Therefore, I explored the possible relationship between the LEM-mediated process and Wnt/PCP signaling. For this analysis, I performed a double-knockdown experiment using a dominant-negative mutant of *Xenopus dishevelled*, *Xdd1* (Sokol, 1996) and xFN-MO. xFN-MO was targeted to the BCR to inhibit the LEM's migratory activity, and *Xdd1* mRNA was targeted to the AM to inhibit the Wnt/PCP pathway (Fig. 3-13A). Importantly, this combined perturbation caused much more severe CE defects than either single perturbation alone (Fig. 3-13B). Based on this result, I propose that proper gastrulation and CE movement of the AM require both the intrinsic function of Wnt/PCP signaling in the AM and the extrinsic supports mediated by the LEM's anterior migration.

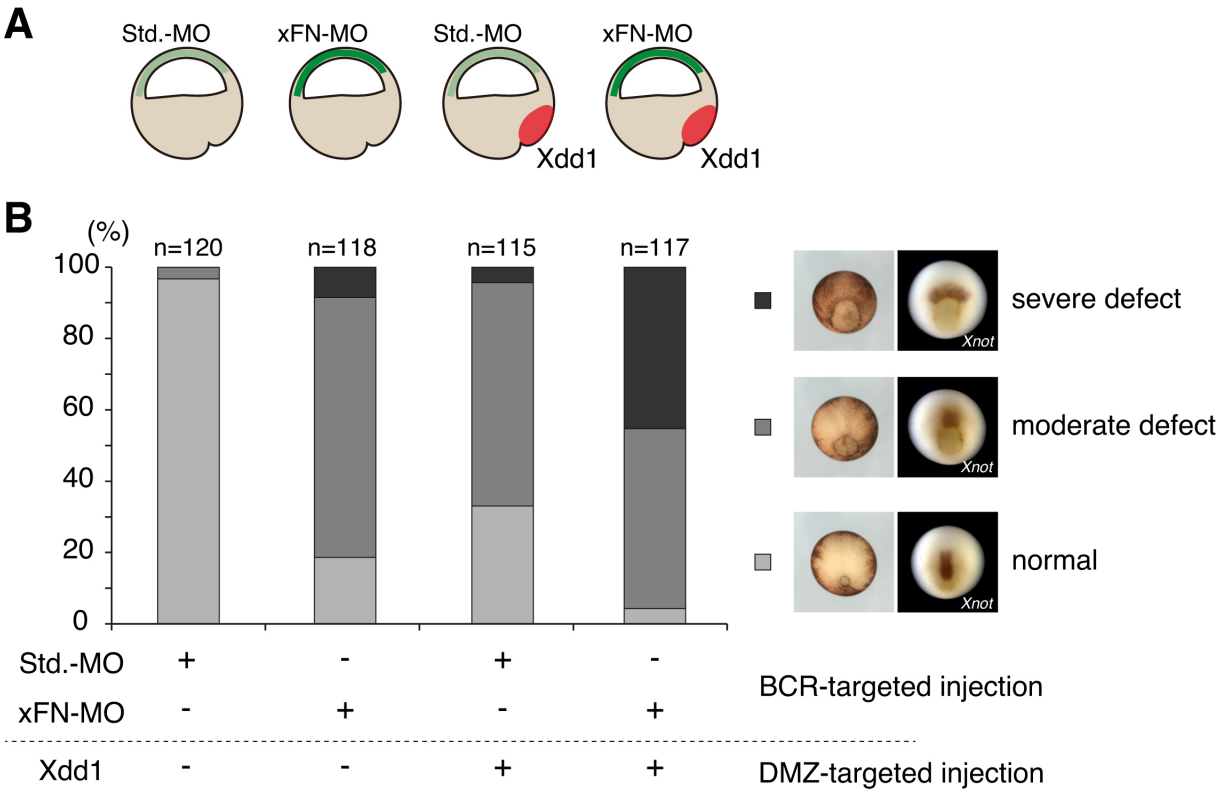

Fig. 3-13 Simultaneous knockdown of LEM's anterior migration and the Wnt/PCP pathway causes severe defects in gastrulation movements.
(A) Scheme of combined knockdown experiment. xFN-MO (0.35 mM) was targeted to the BCR by injection at the 2-cell stage, and *Xdd1* mRNA (250 pg) was targeted to the DMZ by injection at the 4-cell stage.
(B) Quantification of embryos that showed gastrulation defects. Almost all control embryos were normal (*n*=120). The combined knockdown (*n*=117) caused more severe defects than the single injection of xFN-MO (n=118) or Xdd1 (*n*=115).

4. Discussion

In early animal development, gastrulation is one of the important and dynamic morphological processes. In this study, I explored the mechanical factors involved in *Xenopus* gastrulation, and found that the LEM generates physical force by its directional migration at the nano-newton order. I also addressed the possible requirement of directional migration of the LEM for gastrulation movements and proposed that LEM migration and resulting force is important for proper notochord elongation.

4.1 The magnitude of force generated by LEM migration

Using a micro-needle deflection assay, I directly measured the force generated by the directional migration of LEM. Here, I demonstrated that LEM cells migrating as a cohort generate a force of about 40 nN (Fig. 3-2) and the generated force increased in a tissue-size-dependent manner (Fig. 3-3A). Interestingly, according to a recent report (Weber et al., 2012), a single *Xenopus* LEM cell has the potential to generate a pulling force of around 1.5 nN. In my study in which the force generated by about 500 X 500 μm of LEM, which contains hundreds of cells was measured, however, the absolute value was relatively smaller than would be obtained simply by multiplying the 1.5 nN traction force generated by a single cell. For example, for other types of the cells, the force generated was estimated as follows. Fish keratocyte generate traction forces ranging from a minimum of 7.5 nN to a maximum of about 20 nN (Lee et al., 1994). Balaban et al. (Balaban et al., 2001) reported that maximum traction forces as ~20 nN for rat cardiac fibroblast, ~30 nN for human foreskin fibroblast and ~70 nN for rat cardiac myocyte. Other groups reported that forces of chick or human fibroblast as high as 100 nN and 138 nN, respectively (Galbraith et al., 1997; Tymchenko et al., 2007).

For endothelial cells, it was reported that the forces ranges between about 7 and 60 nN (Petronis et al., 2003; Tymchenko et al., 2007). Roure et al. (du Roure et al., 2005) measured the traction force on confluent and monolayer Madin-Darby canine kidney (MDCK) cells and found that maximum traction force is approximately 40 nN exerted by at the monolayer edge. Compared to those values, the LEM-generated force I estimated was relatively small. By the force measurement assay, I found that the value of Force/Area was decreased in a tissue-size dependent manner (Fig. 3-3B). This result implies that the generated force by a single cell is decreased or the generated force is wasted through transmission if the tissue-size is increased. It could be that only a small population of cells in the tissue may be contributing to the force generation. However, the detailed model is not available at this time. Thus, how the LEM cluster of many hundreds of cells generates this relatively small amount of force raises a new question to be asked in the future works. In any case, this apparent difference of the absolute value of generated forces among various types of cells emphasizes the importance of actual measurement of the magnitude of forces especially of tissue movements as I demonstrated in this study.

Of course, there is a possibility that the measurements in this study might under estimate the force in vivo because I cut the most dorsal part of the LEM and measured the force. Thus, the generated force by whole LEM in vivo is probably bigger than the result of in vitro measurement. At the current moment, it is very difficult to measure or estimate the force in embryo with non-destructive methods and I certainly need to wait for the future development of more sophisticated methods. Nevertheless, the migration assay in this study could reconstruct the migratory activity of the LEM in vitro

(Fig.3-1), and thus I believe that my measurements help understanding of the force generation in vivo.

4.2 The LEM migration influence the force distribution of the AM

Using the laser ablation technique, I found that actively migrating tissue could generate a physical force against neighboring tissue (Fig. 3-4). I showed that the recoil of the ablated tissue was greater in the presence of migrating LEM than in its absence or when LEM migrated on an xFN-MO BCR coating. These findings provide direct evidence that the anteriorly migrating LEM stretches the posteriorly-located AM, and thus the force distribution in AM was altered.

Supporting this observations, previous study showed that the part of the DMZ that has already invaginated (the post-involution layer) is under passive tension along the A-P direction at the mid-gastrula stage; if the post-involution layer and the non-involution layer are detached at stage 11 (mid-gastrula), an immediate and extensive contraction and curling of the post-involution layer occurs (Beloussov et al., 2006). The result showing the shrinkage of DMZ tissue after the isolation confirmed this contraction and revealed that the reduction of migratory activity of LEM reduces the shrinkage rate on the AM (Fig. 3-9D-F), suggesting the passive tension on the post-involuted layer at the mid-gastrula stage is come from migrating LEM.

A recent study examined the LEM-AM relationship from a different perspective (Weber et al., 2012). The authors showed that a pulling force from the posterior side induces the anterior migration of LEM cells, and proposed that the trailing AM acts to anchor the mesendoderm by resisting the cell-cell tension generated by the advancing LEM. In

other words, the report suggested that the AM is also subjected to tension from the anteriorly migrating LEM during LEM continues to migrate anteriorly using such resistant force from AM. This study supports my idea that the AM is constantly pulled by the LEM migration. Taken together, I concluded that the migratory activity of the LEM is a source for the A-P directed pulling force on the AM seen in vitro and in vivo.

Incidentally, these interpretations are probably correct at least for the period corresponds to the early-phase of gastrulation which is before active AM elongation occur. I also performed laser ablation experiments in the later stage (St. 12.5-13) when the AM elongated well. I found that the recoil in the AM region was decreased in the later stage compared with the recoils in the early stage (St. 11-11.5) (Fig. 4-1). Interestingly, *Xdd1* mRNA injection that inhibits the AM elongation rescued the tension in the AM (Fig. 4-1). These results suggest that the LEM-mediated tension in the AM region is changed over time by the active AM elongation during gastrulation.

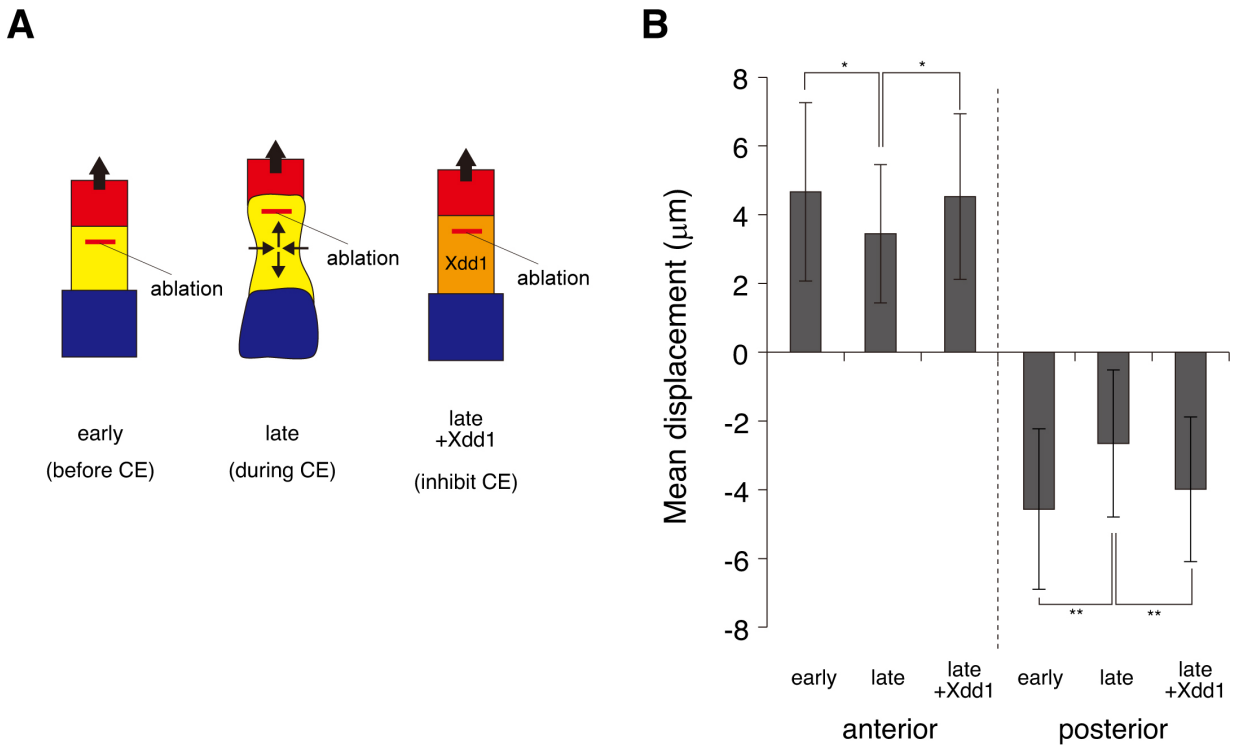

Fig. 4-1 Laser ablation experiments in a later stage

(A) Schematic of the laser ablation experiment. Ablations were carried out after a 2-hour incubation (early stage, St.11-11.5) or 5-hour incubation (late stage, St. 12.5-13). In the late+Xdd1 explant, I injected *Xdd1* mRNA into the AM to inhibit CE movement. Red indicates the LEM, yellow or orange indicates the AM, and blue indicates ectoderm.

(B) The mean displacements calculated from the anterior and posterior regions of ablation line. Positive and negative values of vertical axis indicate anteriorly deformation and posteriorly deformation, respectively. The data of early-explant is the same data set as Fig. 3-8A,C. The late-explants generated less recoils on the anterior and posterior side (n=36, 9 batches, 3.45±2.01 μm (anterior), 2.65±2.14 μm (posterior), mean±s.d.) of the ablation line. The late+Xdd1-explants generated greater recoils on the anterior and posterior side (n=37, 8 batches, 4.53±2.41 μm (anterior), 3.99±2.10 μm (posterior), mean±s.d.) compared with the late-explants. *P<0.05, **P<0.01.

4.3 The functions of LEM migration during *Xenopus* Gastrulation

The in vivo knockdown experiments of the migratory activity of LEM by the regional injection of xFN-MO showed that the reduction of LEM caused abnormal AM elongation (Fig.3-10 3-11). Supporting this observation, previous reports also showed that the anterior migration of LEM affects to normal gastrulation movement and notochord formation. When LEM's migratory activity is impaired by knocking down guidance molecules such as SDF-1 and PDGF, the embryos show gastrulation defects and a shortened A-P axis in later stages (Ataliotis et al., 1995; Fukui et al., 2007; Nagel et al., 2004). In such embryos with reduced LEM migration activity, the notochord fails to extend properly (Ataliotis et al., 1995; Nagel et al., 2004). The authors of these reports speculated that the perturbation of directional molecular cues mainly affects LEM migration, and the CE impairment seen in vivo is an indirect effect. Thus, taking the observation in this study in consideration, these results could also be interpreted as that the LEM supports notochord formation process through its anterior migration in the whole embryo.

Contradictory to these observations, it is well known that the AM can elongate almost normally even if in isolated DMZ explants or in BCR-removed embryos, suggesting that the AM elongation itself does not require the migration of LEM (Keller and Danilchik, 1988; Keller and Jansa, 1992). Furthermore, the sandwich explant of DMZ (keller sandwich), including AM and non-involuting marginal zone (NIMZ), can generate pushing force along A-P direction by its active extension (Moore, 1994). Beloussov et al. reported that the post-involuting layer at stages 13-14 showed extension instead of being contracted after detachment from non-involution layer (Beloussov,

2006). These reports also suggested that the AM at later stages generates pushing force rather than being subjected to passive tension.

These facts complicate the understanding of the function of LEM as to why the AM is affected by the migratory activity of the LEM in vivo if the isolated AM can elongate autonomously. The simplest explanation for this is that the anterior migration of LEM helps the AM to overcome the resistance from surrounding tissues or LEM itself. It was previously proposed that the AM receives resistant forces from passively deformed surrounding tissues such as the vegetal endoderm, the dorsolateral mesoderm, and the dorsolateral epidermis during elongation (Moore et al., 1995). If the LEM does not migrate anteriorly, the LEM act as a drag in front of the AM and the AM therefore cannot generate enough elongation forces to overcome the resistance of dorsal tissues. The reported force AM can generate was up to 600 nN, together with those generated by the parallel extension of the dorsal NIMZ (Moore, 1994). Although the actual magnitude of the single-AM's elongating force is still unclear, there is a possibility that the force generated by AM elongation alone is not sufficient to overcome the resistance. This study suggested that the AM also needs the support of constant anterior-directed LEM migration and resulting force generated, and those two movements cooperate together to overcome the resistance during normal gastrulation. In the situation of isolated explants or BCR-removed embryo, surrounding tissues do not restrict the AM probably, and that is a reason why the AM explant can elongate normally without the LEM and resulting traction force.

The similar interpretation may also be able to explain the cell morphology of AM cells in the LEM migration-defective embryo. At the cellular level, the normal AM cells

polarize along mediolatelal direction as protrusions form at the medial and lateral ends of the cells (Shih and Keller 1992a). This mediolateral protrusive activity is thought to exert traction on adjacent cells each other, and then the cells elongate and align parallel to the mediolateral axis (Shih and Keller 1992a). As the traction forces intercalate the cells, the intercalating cells are thought to generate compression forces against surrounding AM cells (Keller et al., 2008). Ultimately, the compression forces of all of intercalating cells account for the extension forces generated by the AM elongation (Keller et al., 2008; Moore, 1994). Based on these interpretations, there is a possibility that if the LEM fails to migrate anteriorly, the compression force in the AM cells cannot be released along A-P direction and result in excess mechanical resistance arises in the AM cells. In this situation, the AM cells might have a great difficulty in overcoming the overloaded compression force, and thus the cells fail to elongate, align, and intercalate each other. Alternatively, the excess mechanical loading may physically hamper the cellular morphogenesis normally recognized as cell polarization. This interpretation might explain why cell elongation and orientation are apparently disrupted in AM lacking migrating LEM even though Wnt/PCP pathway as revealed by RhoA and Rac1 activity was unaffected (Fig.3-11,12). Therefore, it would be important to examine whether functional polarity of AM cells such as the orientation of protrusion formation and microtubule elongation is indeed maintained in the LEM-defective embryo. In any case, this explanation suggests that at the cell level, the LEM migration may continue to release the compression forces by its pulling force during gastrulation and that makes elongation, alignment, and intercalation easier for the AM cells.

Because the AM shows little directional migration while the LEM actively migrates anteriorly (Fig. 3-1C) and the rate of AM elongation greatly increases in late gastrula (Wilson and Keller, 1991), I presume that the role of LEM migration in releasing the compression to initiate CE is more dominant in early-mid gastrula and the LEM play a less active role by assisting AM elongation force in mid-late gastrula. The results of laser ablation in a later stage also support this model (Fig. 4-1). However, detailed understanding of the mechanism of the transition of these two processes awaits further studies because AM changes its state continuously from non-motile tissue to active elongating tissue during gastrulation. In any case, it would appear that the LEM continues to arrange the force distribution in the dorsal mesoderm region by constant anterior migration since the onset of gastrulation. The results of force measurement and laser ablation of this study strongly suggested that the LEM has an ability to achieve above processes.

Lastly, I would like to propose an additional mechanism in which LEM migration actively participates to the notochord formation in vivo. In the case of cultured cells such as fibroblasts, vascular smooth muscle cells, osteoblasts, and endothelial cells, stretched cells orient their long axis perpendicular to the stretch direction (Goldyn et al., 2010; Goldyn et al., 2009; Morioka et al., 2011; Naruse et al., 1998; Neidlinger-Wilke et al., 2001; Standley et al., 2002), which is consistent with the relationship between the anterior LEM migration and the mediolateral polarization of AM cells. Therefore, it is possible that the directed force could provide cells with polarity information. As reported above, such stretch-induced cell responses often accompany the remodeling of cytoskeletal structures and increment of intracellular Ca^{2+} concentration. Previous study

reported that Ca^{2+} elevation is also required for cell polarization of AM cells during *Xenopus* gastrulation (Shindo et al., 2010; Wallingford et al., 2001). Thus, I further speculated that *Xenopus* AM cells polarize through and Ca^{2+} elevation responding to stretch forces generated by LEM as reported in culture cells. Furthermore, our previous study reveled that the polarized AM cells show mediolateral-directed microtubule growth (Shindo et al., 2008). Another possibility is that such mediolateral alignment of microtubule and other cytoskeleton are induced by stretch forces as also reported in culture cells. Interestingly, several previous reports implied that *Xenopus* AM has a mechanosensitibity; DMZ, including AM, as both suprablastoporal explants and whole embryos, responds to the artificial stretching along the axis perpendicular to the presumptive A-P axis and the cells are reoriented and elongated along the direction of the applied stretch (Beloussov et al., 2006; Troshina and Belousov, 2009). Taken together with these reports, the AM's responsiveness to this external force is a possible mechanism controlling notochord elongation, and the LEM generating force might be used in such system in vivo. Although these speculations remain to be examined, these possible mechanisms might enhance the cell polarization, in addition to the previously proposed mechanism mentioned above.

In summary, I concluded that the LEM adopted these force-mediated mechanisms as an additional layer to the Wnt/PCP pathway to establish robust CE.

4.4 The effect of FN knockdown

The knockdowns of FN and its interacting integrins in *Xenopus* gastrulation were previously reported to retard blastopore closure and CE and to reduce dorsal axis

extension (Davidson et al., 2006; Marsden and DeSimone, 2003; Ramos and DeSimone, 1996). These reports provided evidence that FN in both the BCR and DMZ, including the AM, is required for normal gastrulation and axial extension. The gastrulation defects that I observed in the BCR-specific knockdown of FN by MO were similar to those described in the above reports. Notably, however, in contrast to these reports, I observed aberrant AM morphogenesis even when FN's functions in the AM were not disrupted. Gastrulation and notochord formation were perturbed when only the LEM migratory activity was impaired by FN-knockdown in the BCR; in these embryos, the FN distribution was normal in the DMZ, including the AM. Thus, the present data have provided the further understanding of the role of FN that the presence of FN in the AM is not sufficient for proper CE movement; CE also requires FN served as the lining for the LEM's anterior migration. This might also explain why the knockdown of guidance molecules like PDGF, SDF1, or CXCR4 cause gastrulation defects and abnormal notochord formation in the whole embryo, as reported previously (Ataliotis et al., 1995; Fukui et al., 2007; Nagel et al., 2004).

4.5 Conclusions

The present work clarified where and how much force is generated in the gastrulating embryo, leading us to propose that the anterior migration of LEM is required for the triggering or maintenance of CE movement of the AM mediated by physical forces (Fig. 4-2), and emphasized the importance of physical factors in the regulation of early development. One challenge for future studies is to investigate the remaining possibilities, that whether the AM cells have active-mechanoresponse mechanisms in gastrulation movements. *Xenopus* gastrulation involves distinct types of cell movement, including epiboly of the ectoderm, rotation of the endoderm, radial intercalation, and invagination by bottle cell formation, in addition to LEM migration (Davidson, 2011). The hoop stress around the blastopore lip might also generate force along the A-P direction in *Xenopus* gastrulation, as observed in zebrafish epiboly (Behrndt et al., 2012). Therefore, it will certainly be important to understand the physical nature of the movements occurring in various developmental contexts as well as how the resulting force signals are biologically interpreted by the cells.

The multicellular/tissue movements are observed in a variety of biological processes (Friedl and Gilmour, 2009; Rorth, 2009). The establishment of improved methods for precisely measuring the absolute value of physical forces in other contexts is also important for meaningful comparisons of forces in the future.

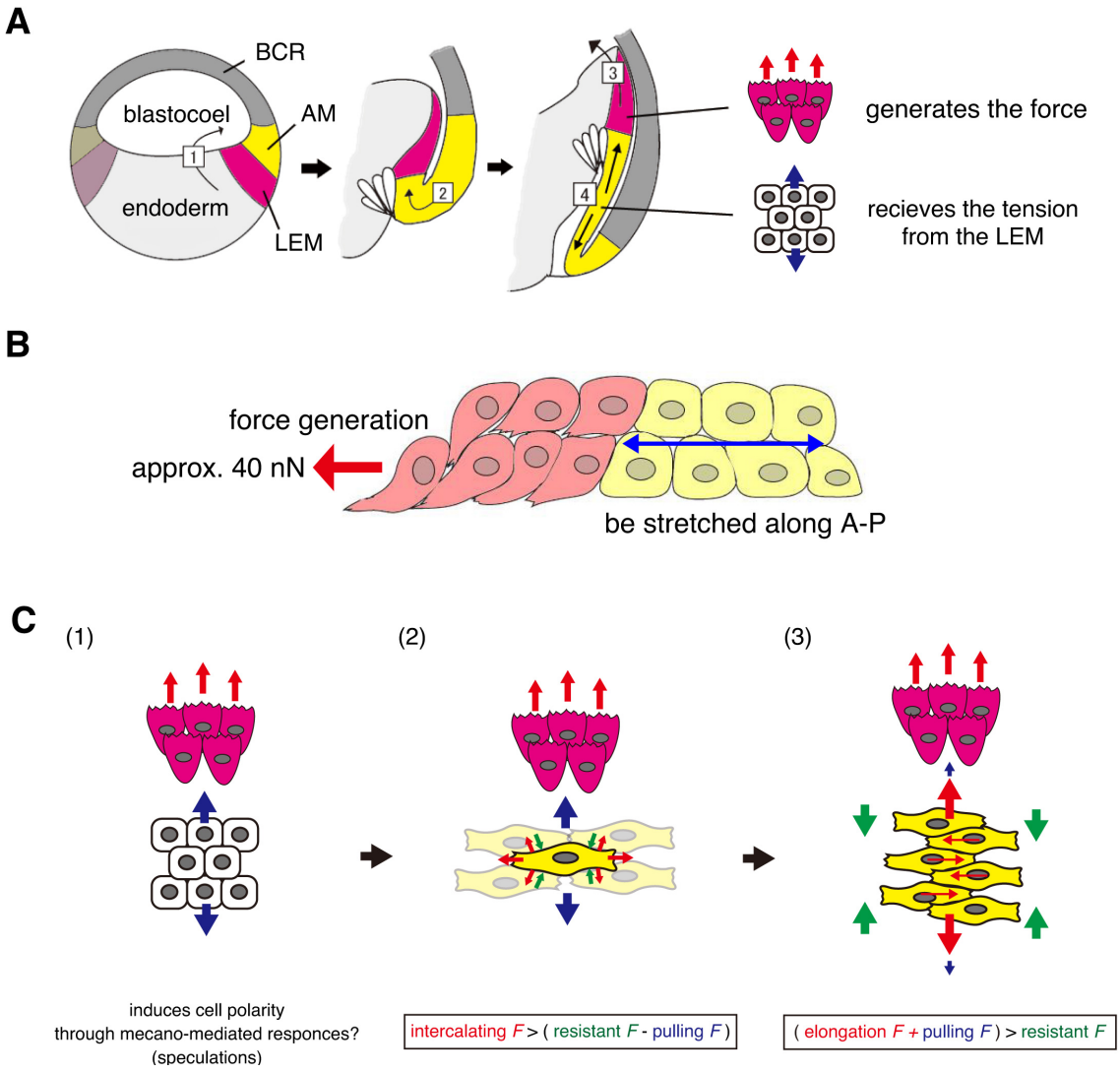

Fig. 4-2 Overview of the functions of LEM migration in gastrulation
(A-B) Interaction between the LEM and the AM. The LEM exerts a pulling force on the AM by its anterior migration. The AM receives the force generated by the LEM and is stretched in the A-P direction.
(C) Model of the functions of the migrating LEM *in vivo*. The role of the pulling force from the LEM could aid CE of the AM: 1) The tensile forces imposed on the AM and may induce mechanical-mediated responses that acts in concert with other pathways supporting cell polarization. 2) Exerting a tensile force on the AM mechanically acts internally in the mechanism of CE by reducing the local compressive forces preventing them from intercalating between one another, and making it easier for the cells to elongate and align. 3) The LEM moves out of the way of the AM elongation. At the same time, the LEM still exerts a tension on the anterior end of the AM to reduce the compressive load on the actively extending AM and make it easier for the AM to overcome the resistant forces from surrounding tissues.
Red arrows indicate active forces and blue arrows indicate passive force. Green arrows indicate prospective resistant forces.

5.References

Aigouy, B., Farhadifar, R., Staple, D.B., Sagner, A., Roper, J.C., Julicher, F., Eaton, S., 2010. Cell flow reorients the axis of planar polarity in the wing epithelium of Drosophila. *Cell* 142, 773-786.

Ataliotis, P., Symes, K., Chou, M.M., Ho, L., Mercola, M., 1995. PDGF signalling is required for gastrulation of *Xenopus laevis*. *Development* 121, 3099-3110.

Balaban, N.Q., Schwarz, U.S., Riveline, D., Goichberg, P., Tzur, G., Sabanay, I., Mahalu, D., Safran, S., Bershadsky, A., Addadi, L., Geiger, B., 2001. Force and focal adhesion assembly: a close relationship studied using elastic micropatterned substrates. *Nat. Cell. Biol.* 3, 466-472.

Behrndt, M., Salbreux, G., Campinho, P., Hauschild, R., Oswald, F., Roensch, J., Grill, S.W., Heisenberg, C.P., 2012. Forces driving epithelial spreading in zebrafish gastrulation. *Science* 338, 257-260.

Beloussov, L.V., Luchinskaya, N.N., Ermakov, A.S., Glagoleva, N.S., 2006. Gastrulation in amphibian embryos, regarded as a succession of biomechanical feedback events. *Int. J. Dev. Biol.* 50, 113-122.

Berger, C.D., Marz, M., Kitzing, T.M., Grosse, R., Steinbeisser, H., 2009. Detection of activated Rho in fixed *Xenopus* tissue. *Dev. Dyn.* 238, 1407-1411.

Boucaut, J.C., Darribere, T., 1983. Fibronectin in early amphibian embryos. Migrating mesodermal cells contact fibronectin established prior to gastrulation. *Cell and tissue research* 234, 135-145.

Davidson, L.A., 2011. Embryo mechanics: balancing force production with elastic resistance during morphogenesis. *Current topics in developmental biology* 95, 215-241.

Davidson, L.A., Hoffstrom, B.G., Keller, R., DeSimone, D.W., 2002. Mesendoderm extension and mantle closure in *Xenopus laevis* gastrulation: combined roles for integrin alpha(5)beta(1), fibronectin, and tissue geometry. *Dev. Biol.* 242, 109-129.

Davidson, L.A., Keller, R., DeSimone, D.W., 2004. Assembly and remodeling of the fibrillar fibronectin extracellular matrix during gastrulation and neurulation in *Xenopus laevis*. Dev. Dyn. 231, 888-895.

Davidson, L.A., Marsden, M., Keller, R., Desimone, D.W., 2006. Integrin alpha5beta1 and fibronectin regulate polarized cell protrusions required for *Xenopus* convergence and extension. *Current biology* 16, 833-844.

du Roure, O., Saez, A., Buguin, A., Austin, R.H., Chavrier, P., Silberzan, P., Ladoux, B., 2005. Force mapping in epithelial cell migration. *Proc. Natl. Acad. Sci. USA* 102, 2390-2395.

Engler, A.J., Sen, S., Sweeney, H.L., Discher, D.E., 2006. Matrix elasticity directs stem cell lineage specification. *Cell* 126, 677-689.

Fink, J., Carpi, N., Betz, T., Betard, A., Chebah, M., Azioune, A., Bornens, M., Sykes, C., Fetler, L., Cuvelier, D., Piel, M., 2011. External forces control mitotic spindle positioning. *Nat. Cell. Biol.* 13, 771-778.

Friedl, P., Gilmour, D., 2009. Collective cell migration in morphogenesis, regeneration and cancer. *Nat. Rev. Mol. Cell Biol.* 10, 445-457.

Fukui, A., Goto, T., Kitamoto, J., Homma, M., Asashima, M., 2007. SDF-1 alpha regulates mesendodermal cell migration during frog gastrulation. *Biochemical and biophysical research communications* 354, 472-477.

Galbraith, C.G., Sheetz, M.P., 1997. A micromachined device provides a new bend on fibroblast traction forces. *Proc. Natl. Acad. Sci. USA* 94, 9114-9118.

Goda, T., Takagi, C., Ueno, N., 2009. *Xenopus* Rnd1 and Rnd3 GTP-binding proteins are expressed under the control of segmentation clock and required for somite formation. *Dev. Dyn.* 238, 2867-2876.

Goldyn, A.M., Kaiser, P., Spatz, J.P., Ballestrem, C., Kemkemer, R., 2010. The kinetics of force-induced cell reorganization depend on microtubules and actin. *Cytoskeleton (Hoboken)* 67, 241-250.

Goldyn, A.M., Rioja, B.A., Spatz, J.P., Ballestrem, C., Kemkemer, R., 2009. Force-induced cell polarisation is linked to RhoA-driven microtubule-independent focal-adhesion sliding. *Journal of cell science* 122, 3644-3651.

Habas, R., Dawid, I.B., He, X., 2003. Coactivation of Rac and Rho by Wnt/Frizzled signaling is required for vertebrate gastrulation. *Genes & development* 17, 295-309.

Habas, R., Kato, Y., He, X., 2001. Wnt/Frizzled activation of Rho regulates vertebrate gastrulation and requires a novel Formin homology protein Daam1. *Cell* 107, 843-854.

Hopwood, N.D., Pluck, A., Gurdon, J.B., 1989. MyoD expression in the forming somites is an early response to mesoderm induction in *Xenopus* embryos. *The EMBO journal* 8, 3409-3417.

Ingber, D.E., 2006. Cellular mechanotransduction: putting all the pieces together again. *FASEB journal* 20, 811-827.

Ives, C.L., Eskin, S.G., McIntire, L.V., 1986. Mechanical effects on endothelial cell morphology: in vitro assessment. *In vitro cellular & developmental biology : journal of the Tissue Culture Association* 22, 500-507.

Jaalouk, D.E., Lammerding, J., 2009. Mechanotransduction gone awry. *Nat. Rev. Mol. Cell Biol.* 10, 63-73.

Joshi, S.D., von Dassow, M., Davidson, L.A., 2010. Experimental control of excitable embryonic tissues: three stimuli induce rapid epithelial contraction. *Experimental cell research* 316, 103-114.

Keller, R., 2002. Shaping the vertebrate body plan by polarized embryonic cell movements. *Science* 298, 1950-1954.

Keller, R., Danilchik, M., 1988. Regional expression, pattern and timing of convergence and extension during gastrulation of *Xenopus laevis*. *Development* 103, 193-209.

Keller, R., Davidson, L., Edlund, A., Elul, T., Ezin, M., Shook, D., Skoglund, P., 2000. Mechanisms of convergence and extension by cell intercalation. *Philosophical transactions of the Royal Society of London. Series B, Biological sciences* 355, 897-922.

Keller, R., Davidson, L.A., Shook, D.R., 2003. How we are shaped: the biomechanics of gastrulation. *Differentiation; research in biological diversity* 71, 171-205.

Keller, R., Jansa, S., 1992. *Xenopus* Gastrulation without a blastocoel roof. *Dev. Dyn.* 195, 162-176.

Keller, R., Shook, D., Skoglund, P., 2008. The forces that shape embryos: physical aspects of convergent extension by cell intercalation. *Physical biology* 5, 015007.

Kiehart, D.P., Galbraith, C.G., Edwards, K.A., Rickoll, W.L., Montague, R.A., 2000. Multiple forces contribute to cell sheet morphogenesis for dorsal closure in Drosophila. *The Journal of cell biology* 149, 471-490.

Klein, E.A., Yin, L., Kothapalli, D., Castagnino, P., Byfield, F.J., Xu, T., Levental, I., Hawthorne, E., Janmey, P.A., Assoian, R.K., 2009. Cell-cycle control by physiological matrix elasticity and in vivo tissue stiffening. *Current biology* 19, 1511-1518.

Kwan, K.M., Kirschner, M.W., 2003. Xbra functions as a switch between cell migration and convergent extension in the *Xenopus* gastrula. *Development* 130, 1961-1972.

Lecuit, T., Lenne, P.F., Munro, E., 2011. Force generation, transmission, and integration during cell and tissue morphogenesis. *Annual review of cell and developmental biology* 27, 157-184.

Lee, G., Hynes, R., Kirschner, M., 1984. Temporal and spatial regulation of fibronectin in early *Xenopus* development. *Cell* 36, 729-740.

Lee, J., Leonard, M., Oliver, T., Ishihara, A., Jacobson, K., 1994. Traction forces generated by locomoting keratocytes. *The Journal of cell biology* 127, 1957-1964.

Lo, C.M., Wang, H.B., Dembo, M., Wang, Y.L., 2000. Cell movement is guided by the rigidity of the substrate. *Biophysical journal* 79, 144-152.

Mammoto, T., Ingber, D.E., 2010. Mechanical control of tissue and organ development. *Development* 137, 1407-1420.

Marsden, M., DeSimone, D.W., 2003. Integrin-ECM interactions regulate cadherin-dependent cell adhesion and are required for convergent extension in *Xenopus*. *Current biology* 13, 1182-1191.

Martin, A.C., Gelbart, M., Fernandez-Gonzalez, R., Kaschube, M., Wieschaus, E.F., 2010. Integration of contractile forces during tissue invagination. *The Journal of cell biology* 188, 735-749.

Matsumoto, T., Goto, T., Furukawa, T., Sato, M., 2004. Residual stress and strain in the lamellar unit of the porcine aorta: experiment and analysis. *Journal of biomechanics* 37, 807-815.

Moore, S.W., 1994. A fiber optic system for measuring dynamic mechanical properties of embryonic tissues. *IEEE transactions on bio-medical engineering* 41, 45-50.

Moore, S.W., Keller, R.E., Koehl, M.A., 1995. The dorsal involuting marginal zone stiffens anisotropically during its convergent extension in the gastrula of *Xenopus* laevis. *Development* 121, 3131-3140.

Morioka, M., Parameswaran, H., Naruse, K., Kondo, M., Sokabe, M., Hasegawa, Y., Suki, B., Ito, S., 2011. Microtubule dynamics regulate cyclic stretch-induced cell alignment in human airway smooth muscle cells. *PloS one* 6, e26384.

Morita, H., Kajiura-Kobayashi, H., Takagi, C., Yamamoto, T.S., Nonaka, S., Ueno, N., 2012. Cell movements of the deep layer of non-neural ectoderm underlie complete neural tube closure in *Xenopus*. *Development* 139, 1417-1426.

Morita, H., Nandadasa, S., Yamamoto, T.S., Terasaka-Iioka, C., Wylie, C., Ueno, N., 2010. Nectin-2 and N-cadherin interact through extracellular domains and induce

apical accumulation of F-actin in apical constriction of *Xenopus* neural tube morphogenesis. *Development* 137, 1315-1325.

Nagayama, K., Matsumoto, T., 2008. Contribution of actin filaments and microtubules to quasi-in situ tensile properties and internal force balance of cultured smooth muscle cells on a substrate. *American journal of physiology. Cell physiology* 295, C1569-1578.

Nagel, M., Tahinci, E., Symes, K., Winklbauer, R., 2004. Guidance of mesoderm cell migration in the *Xenopus* gastrula requires PDGF signaling. *Development* 131, 2727-2736.

Naruse, K., Yamada, T., Sokabe, M., 1998. Involvement of SA channels in orienting response of cultured endothelial cells to cyclic stretch. *The American journal of physiology* 274, H1532-1538.

Neidlinger-Wilke, C., Grood, E.S., Wang, J.-C., Brand, R.A., Claes, L., 2001. Cell alignment is induced by cyclic changes in cell length: studies of cells grown in cyclically stretched substrates. *Journal of orthopaedic research : official publication of the Orthopaedic Research Society* 19, 286-293.

Nieuwkoop, P.D., Faber, J., 1967. Normal Table of *Xenopus laevis* (Daudin). North-Holland, Amsterdam.

Petronis, S., Gold, J., Kasemo, B., 2003. Microfabricated force-sensitive elastic substrates for investigation of mechanical cell–substrate interactions. *Journal of Micromechanics and Microengineering* 13.

Ramos, J.W., DeSimone, D.W., 1996. *Xenopus* embryonic cell adhesion to fibronectin: position-specific activation of RGD/synergy site-dependent migratory behavior at gastrulation. *The Journal of cell biology* 134, 227-240.

Rorth, P., 2009. Collective cell migration. *Annual review of cell and developmental biology* 25, 407-429.

Sater, A.K., Steinhardt, R.A., Keller, R., 1993. Induction of neuronal differentiation by planar signals in *Xenopus* embryos. *Dev. Dyn.* 197, 268-280.

Shih, J., Keller, R., 1992a. Cell motility driving mediolateral intercalation in explants of *Xenopus laevis*. *Development* 116, 901-914.

Shih, J., Keller, R., 1992b. Patterns of cell motility in the organizer and dorsal mesoderm of *Xenopus laevis*. *Development* 116, 915-930.

Shindo, A., Hara, Y., Yamamoto, T.S., Ohkura, M., Nakai, J., Ueno, N., 2010. Tissue-tissue interaction-triggered calcium elevation is required for cell polarization during *Xenopus* gastrulation. *PloS one* 5, e8897.

Shindo, A., Yamamoto, T.S., Ueno, N., 2008. Coordination of cell polarity during *Xenopus* gastrulation. *PloS one* 3, e1600.

Sokol, S.Y., 1996. Analysis of Dishevelled signalling pathways during *Xenopus* development. *Current biology* 6, 1456-1467.

Solnica-Krezel, L., Sepich, D.S., 2012. Gastrulation: making and shaping germ layers. *Annual review of cell and developmental biology* 28, 687-717.

Standley, P.R., Cammarata, A., Nolan, B.P., Purgason, C.T., Stanley, M.A., 2002. Cyclic stretch induces vascular smooth muscle cell alignment via NO signaling. *American journal of physiology. Heart and circulatory physiology* 283, H1907-1914.

Suzuki, M., Hara, Y., Takagi, C., Yamamoto, T.S., Ueno, N., 2010. MID1 and MID2 are required for *Xenopus* neural tube closure through the regulation of microtubule organization. *Development* 137, 2329-2339.

Tada, M., Concha, M.L., Heisenberg, C.P., 2002. Non-canonical Wnt signalling and regulation of gastrulation movements. *Seminars in cell & developmental biology* 13, 251-260.

Tada, M., Heisenberg, C.P., 2012. Convergent extension: using collective cell migration and cell intercalation to shape embryos. *Development* 139, 3897-3904.

Tahinci, E., Symes, K., 2003. Distinct functions of Rho and Rac are required for convergent extension during *Xenopus* gastrulation. *Dev. Biol.* 259, 318-335.

Tan, J.L., Tien, J., Pirone, D.M., Gray, D.S., Bhadriraju, K., Chen, C.S., 2003. Cells lying on a bed of microneedles: an approach to isolate mechanical force. *Proc. Natl. Acad. Sci. USA* 100, 1484-1489.

Trepat, X., Wasserman, M.R., Angelini, T.E., Millet, E., Weitz, D.A., Butler, J.P., Fredberg, J.J., 2009. Physical forces during collective cell migration. *Nat. Physics* 5, 426-430.

Troshina, T.G., Belousov, L.V., 2009. Mechanodependent cell movements in the axial rudiments of *Xenopus* gastrulae. *Russian Journal of Developmental Biology* 40, 115-120.

Tymchenko, N., Wallentin, J., Petronis, S., Bjursten, L.M., Kasemo, B., Gold, J., 2007. A novel cell force sensor for quantification of traction during cell spreading and contact guidance. *Biophysical journal* 93, 335-345.

Wacker, S., Brodbeck, A., Lemaire, P., Niehrs, C., Winklbauer, R., 1998. Patterns and control of cell motility in the *Xenopus* gastrula. *Development* 125, 1931-1942.

Wallingford, J.B., Ewald, A.J., Harland, R.M., Fraser, S.E., 2001. Calcium signaling during convergent extension in *Xenopus*. *Current biology* 11, 652-661.

Wallingford, J.B., Fraser, S.E., Harland, R.M., 2002. Convergent extension: the molecular control of polarized cell movement during embryonic development. *Dev. Cell* 2, 695-706.

Wallingford, J.B., Rowning, B.A., Vogeli, K.M., Rothbacher, U., Fraser, S.E., Harland, R.M., 2000. Dishevelled controls cell polarity during *Xenopus* gastrulation. *Nature* 405, 81-85.

Wang, Y., Steinbeisser, H., 2009. Molecular basis of morphogenesis during vertebrate gastrulation. *Cellular and molecular life sciences* 66, 2263-2273.

Weber, G.F., Bjerke, M.A., DeSimone, D.W., 2012. A mechanoresponsive cadherin-keratin complex directs polarized protrusive behavior and collective cell migration. *Dev. Cell* 22, 104-115.

Wilson, P., Keller, R., 1991. Cell rearrangement during gastrulation of *Xenopus*: direct observation of cultured explants. *Development* 112, 289-300.

Winklbauer, R., 1990. Mesodermal cell migration during *Xenopus* gastrulation. *Dev. Biol.* 142, 155-168.

Winklbauer, R., Keller, R.E., 1996. Fibronectin, mesoderm migration, and gastrulation in *Xenopus*. *Dev. Biol.* 177, 413-426.

Winklbauer, R., Nagel, M., 1991. Directional mesoderm cell migration in the *Xenopus* gastrula. *Dev. Biol.* 148, 573-589.

Winklbauer, R., Schurfeld, M., 1999. Vegetal rotation, a new gastrulation movement involved in the internalization of the mesoderm and endoderm in *Xenopus*. *Development* 126, 3703-3713.

Wozniak, M.A., Chen, C.S., 2009. Mechanotransduction in development: a growing role for contractility. *Nat. Rev. Mol. Cell Biol.* 10, 34-43.

Yamamoto, T.S., Takagi, C., Hyodo, A.C., Ueno, N., 2001. Suppression of head formation by Xmsx-1 through the inhibition of intracellular nodal signaling. *Development* 128, 2769-2779.

Zhang, H., Labouesse, M., 2012. Signalling through mechanical inputs - a coordinated process. *Journal of cell science* 125, 3039-3049.

Acknowledgements

I would like to thank my supervisor Professor Naoto Ueno for giving me this opportunity to study as a Ph.D. student in his laboratory. I want to thank Dr, Suzuki Makoto, and Takamasa S. Yamamoto for a helpful contribution to this work as co-workers. Their supports for experiments were indispensable for accomplishing this work. I express my gratitude to Professor Takeo Matsumoto, Dr. Kazuaki Nagayama in Nagoya Institute of Technology for collaborating with me in this work by giving a suggestions and technical supports. I thank Dr. Lance A. Davidson for valuable discussions and technical advice. I would like to thank Dr. Benoit Aigouy (MPI-CBG) for providing us "Packing Analyzer" the image analysis software. I would like to thank Dr. Shigenori Nonaka (NIBB) for the explant-tracing macro of ImageJ. I thank Spectrography and Bioimaging Facility, NIBB Core Research Facilities for technical support.

Funding from the Japan Society for the Promotion of Science (JSPS) Research Fellowships for Young Scientists supported this work.

I am deeply grateful to all the people in Division of Morphogenesis in NIBB for assisting me with experiments and daily life.